PACIFIC EARTHQUAKE ENGINEERING RESEARCH CENTER

Performance-Based Evaluation of Exterior Reinforced Concrete Building Joints for Seismic Excitation

Chandra Clyde
Chris P. Pantelides
Lawrence D. Reaveley
University of Utah

A report on research conducted under
Grant No. SA1810JB from the National Science Foundation

PEER 2000/05
JULY 2000

Performance-Based Evaluation of Exterior Reinforced Concrete Building Joints for Seismic Excitation

Chandra Clyde
Research Assistant
University of Utah

Chris P. Pantelides
Professor of Civil Engineering
University of Utah

Lawrence D. Reaveley
Professor of Civil Engineering
University of Utah

A report on research conducted under
grant no. SA1810JB from the National Science Foundation

PEER Report 2000/05
Pacific Earthquake Engineering Research Center
College of Engineering
University of California, Berkeley

July 2000

ABSTRACT

Reinforced concrete (RC) buildings that were built in the 1960s behave in a nonductile manner and do not meet current seismic design criteria. In this report, beam-column joints of such nonductile buildings are investigated using several performance-based criteria. Four half-scale RC exterior joints were tested to investigate their behavior in a shear-critical mode. The joints were subjected to quasi-static cyclic loading, and their performance was examined in terms of lateral load capacity, drift, axial load reduction in the column at high levels of drift, joint shear strength, ductility, shear angle, residual strength, and other PEER established performance criteria. Two levels of axial compression load in the columns were investigated, and their influence on the performance of the joint are discussed.

ACKNOWLEDGMENTS

The research presented in this report was performed at the University of Utah. This work was supported in part by the Pacific Earthquake Engineering Research Center through the Earthquake Engineering Research Centers Program of the National Science Foundation under Award number EEC-9701568. In-kind contribution made by Eagle Precast Company is greatly appreciated, as are the efforts of those individuals who helped on this project.

CONTENTS

LIST OF FIGURES

LIST OF TABLES

1 Introduction

Reinforced concrete buildings that were built in the 1960s have limited ductility and several deficiencies that prevent them from meeting current seismic design criteria. In this research, exterior beam-column joints of plane multistory frames are investigated using several performance-based criteria. The effect of the axial compression load in the column, on the joint performance at high levels of drift is investigated.

1.1 LITERATURE REVIEW

Research on the seismic performance of RC building joints has been carried out in the last four decades. The majority of this research has emphasized the improvement of the performance of these joints through new design concepts and improved details such as joint hoops. The emphasis of the present research is the evaluation of the seismic performance of existing non-ductile buildings, which is the focus of current PEER efforts.

Townsend and Hanson performed research on 22 reinforced concrete beam-column T-shaped connections. These specimens were tested under column axial tension ($0.25f'_cA_g$), column axial compression ($0.15f'_cA_g$), and no column load. It was shown that increased column tension causes the moment capacity to decrease more rapidly, representing a faster rate of concrete deterioration than the specimens with no column load or column compressive load (Townsend 1977).

The effect of column axial load was investigated in an analytical study of 57 exterior beam-column joint tests. The relationship between the maximum joint shear stress factor and the nominal column axial stress (normalized by f'_c) was sought with respect to hinging and shear failures. For the limited amount of available experimental data, no discernable correlation was established between the two variables. It was concluded that deformability, rather than strength, would be affected by axial load. In the same study, a finite element model was developed to study the effect of several parameters on the shear behavior of interior and exterior joints. The calculated field pattern of principal compressive stresses agrees with the damage observed in the present tests even though no steel hoops were used in the present joints (Pantazopoulou 1994).

Limited experimental evidence suggests that increasing column axial load tends to reduce the total lateral drift at yield (Kurose 1987). Beres et al. (1992) reported on the shear strength of joints without reinforcement. Although some researchers report that increased column axial load results in increased shear strength, the data do not show a significant trend.

In a study of New Zealand and American concrete structural design codes, Park states that the shear strength of beam-column joints in the New Zealand Standard NZS 3101 (1995) is based on the contribution of two mechanisms. The first mechanism is a diagonal compression concrete strut that transfers the compression forces from the beam and column actions without the aid of shear reinforcement. The second mechanism is a stress mechanism that transfers bond forces from the longitudinal bars utilizing horizontal and vertical joint shear reinforcement and concrete struts. It is clear that the NZS 3101 regards the transverse reinforcement in beam-column joints as being placed mainly to resist joint shear. By contrast, the American Concrete Institute ACI 318-95 Code regards the reinforcement in beam-column joints more as confining reinforcement governed by the quantity placed in the adjacent ends of the columns (Park 1997).

Park's study also states that the 1995 version of the New Zealand Standard recognizes that part of the bond forces from the longitudinal beam bars passing through the joint core will be transferred by the diagonal compression strut mechanism. Because of bond deterioration, some bar forces are being transferred directly to the end of the diagonal compression strut. It is accepted that the single diagonal compression strut can transfer a more significant part of the joint shear. Consequently, the quantity of shear reinforcement required in the joint core is significantly lower in the NZS 3101 (1995) than that required by the earlier NZS 3101 (1982). This study also states that bond deterioration was observed only at higher axial load corresponding to $0.25f'_cA_g$ (Park 1997).

The behavior of two exterior reinforced concrete beam-column joins with low axial column load has been investigated by Megget (1974). The variable parameter was the addition of transverse beam stubs to the joint specimen. The column length was the distance between the points of contraflexure. The length of the beam was chosen so that when the negative yield moment was reached at the column face, the specimen's beam shear at that position would be approximately equal to the actual structure's shear when negative yielding in the beam occurred. The diagonal cracks in the joint formed from one corner to the diagonally opposite corner. At

3% drift, joint diagonal cracks as large as 5 mm were observed. The nominal shear stress at the first cracking was between $0.15f'_c$ and $0.17f'_c$. It was felt that the presence of the transverse beam reinforcing had little effect in confining the joint region. The presence of the transverse beams greatly contributed to the confinement of the joint core concrete, however, thus allowing a ductile plastic hinge to form entirely in the beam rather than in the joint region. However, it is uncertain whether this benefit will still exist in the actual case where the transverse beams will have cracked along their beam-column junctions during a non-unidirectional earthquake.

Of the eight specimens tested in another investigation (Uzumeri 1977), three exterior reinforced concrete beam-column joints were tested under constant axial compressive load equal to $0.42f'_cA_g$. The presence of this axial load is of help at the early stages of loading. However, at the latter stages when the concrete core acts as a series of struts, it is postulated that the large axial load may be detrimental rather than helpful. The three specimens were not reinforced in the joint area. Two of the specimens contained a transverse stub beam on one side of the column, whereas the third specimen had no transverse beams. Load reversals after bond loss caused large deformations in the concrete, which resulted in splitting along column bars and anchorage failure of the beam steel. In all three cases, the beam remained intact while the joint rapidly deteriorated with increasing imposed displacements. The joints without transverse reinforcement were able to provide anchorage for the beam steel to the extent that between 92% and 98% of the theoretical ultimate moment capacity of the beams was reached. The joint was unable, however, to sustain the anchorage of the beam steel in cycles subsequent to this load level.

An experimental study of three exterior beam-column joints indicates that the horizontal joint shear reinforcement may be reduced considerably (Paulay and Scarpas 1981). However, the vertical shear reinforcement (i.e., intermediate column bars) was the same in all units. The effect of the axial load was studied in one of the units when it was reduced from $0.15f'_cA_g$ to $0.075f'_cA_g$; this resulted in a dramatic reduction of the stiffness, strength, and energy dissipation of the specimen in the later loading cycle.

In an experimental study of 14 exterior beam-column joints, it was found that axial load changes during seismic loading produces significant deterioration in the joint resistance (Tsonos 1995). High horizontal and/or vertical joint shear stresses exceeding $12\sqrt{f'_c}$ (psi) or $1\sqrt{f'_c}$ (MPa) resulted in significant deterioration in the beam-column joint load-carrying capacity. It was found that the P-Δ effect could be ignored in detailing exterior beam-column connections.

Pantazapoulou and Bonacci investigated the mechanics of beam-column joints in laterally loaded frames (1992). The formulation establishes compatibility of strain and stress equilibrium. It is shown that the shear strength of a joint depends on the usable compressive strength of concrete. It is also concluded that joint shear strength could decrease with increasing column axial force. It was found that, in addition to bond failure, joint capacity could be limited by crushing along the principal diagonal or by yielding of vertical reinforcement after hoop yield.

Six, three-quarter scale exterior beam-to-column connection subassemblies were tested under simulated earthquake loads by Durrani and Zerbe (1987). Four of the specimens contained a slab and transverse beams, one contained transverse beams but no slab, and one had neither transverse beams nor a slab. It was found that the presence of a slab in exterior beam-to-column connections increased the negative flexural capacity of beams by as much as 70%. By ignoring the contribution of the slab, the flexural strength of beams is substantially underestimated. The transverse beams were effective in confining the joint before experiencing torsional cracks. Once the transverse beams reached their torsional cracking strength, their ability to confine the joint diminished. In situations where the cracking of transverse beams is expected, they may not be relied upon for confining the joint.

Ehsani and Wight presented the results of six exterior reinforced concrete beam-column subassemblages that were tested in cyclic loading (1985). It was determined that in order to avoid formation of plastic hinges in the joint the flexural strength ratio should be no less than 1.4. The maximum joint shear stress in exterior connections should be limited to $12\sqrt{f'_c}$ psi ($1.0\sqrt{f'_c}$ MPa) to reduce excessive joint damage, column bar slippage, and beam bar pullout. It was found that in cases where the flexural strength ratio, the joint shear stress, or the anchorage requirements are significantly more conservative than the limits of the recommendations, the amount of joint transverse reinforcement could be safely reduced.

1.2 OBJECTIVE

Reinforced concrete frames can achieve ductile behavior provided that brittle failure of structural elements and instability can be prevented in severe earthquakes. The design and detailing of beam-column joints is important in achieving satisfactory performance of reinforced concrete frames. The design should be able to (1) prevent brittle failure of the joint, (2) maintain integrity of the joint so that the ultimate strength of the connecting beams and columns can be developed and the axial load-carrying capacity of the column can be sustained, and (3) reduce joint stiffness degradation by minimizing cracking of the joint concrete and preventing loss of bond between the concrete and longitudinal beam and column reinforcement. Joints in existing structures built before the development of current design guidelines such as ACI 352R-91 (1991) do not conform to the current requirements (ACI SP-123 1991). The research described targets the performance of exterior joints in existing nonductile RC frame structures in order to establish their adequacy in terms of performance-based criteria. While all components of the specimen performance were evaluated, the main focus of the study is shear in the joint region. Another objective of this research is to determine the effect of high drift on the axial load in the column. A final objective is the evaluation of the influence of the column axial load on the shear strength of the joint.

This report gives a detailed description of the simulated seismic tests performed on four RC beam-column building joints. Performance-based evaluation and suggested performance levels for this type of joint are presented. A comparison of the shear angle with established performance-based guidelines for buildings found in the FEMA *273 Guidelines for the Seismic Rehabilitation of Buildings* (BSSC 1997) is discussed, as well as the shear strength coefficient with respect to the FEMA 273 *Guidelines* and the ACI Code.

2 Test Specimens

2.1 DESCRIPTION OF TEST SPECIMENS

A typical exterior beam-column joint in a reinforced concrete frame building built in 1964 was chosen as a model for this project. The overall dimensions of the original joint were reduced by half, and reinforcing details were reduced based on shear stress calculations. The longitudinal reinforcement in the beam was increased to prevent early degradation of the beam, forcing a shear mode of failure in the joint. There is no transverse reinforcement within the joint core, and the beam longitudinal bars are not adequately anchored in the connection. In addition, the lap splice length and confining reinforcement details are inadequate according to current criteria (ACI 352, 1991).

2.2 MATERIAL PROPERTIES

2.2.1 Concrete

The original design of the specimens called for a concrete strength of 4000 psi (27.6 MPa). However, due to resource restrictions higher strengths were achieved. There was also some variation in concrete strength between specimens. The data resulting from the tests indicate that these variations did not significantly affect the results of the tests. Table 2.1 shows the concrete compressive strength of each specimen.

Table 2.1 Concrete Strength of Specimens

Test No.	f'c psi (MPa)
2	6700 (46.2)
4	5940 (41.0)
5	5370 (37.0)
6	5823 (40.1)

2.2.2 Steel Reinforcement

Three sizes of deformed steel rebar were used for reinforcement in the specimens. Number 7 and 9 bars were used as longitudinal reinforcement in the column and beam, respectively. Stirrups in the beam and column ties were #3 bars. The ultimate (F_u) and yield (F_y) strengths of the reinforcement used in the tests are shown in Table 2.2 below.

Table 2.2 Steel Reinforcement Strength

Reinforcement Type	Bar Size	F_u ksi (MPa)	F_y ksi (MPa)
beam longitudinal	9	108.2 (746.0)	65.9 (454.4)
column longitudinal	7	107.6 (741.9)	68.1 (469.5)
stirrups/ties	3	94.9 (654.3)	62.0 (427.5)

2.3 CONSTRUCTION OF TEST SPECIMENS

All four beam-column specimens had exactly the same dimensions and detailing. The specimen dimensions and reinforcement details are shown in Fig. 2.1.

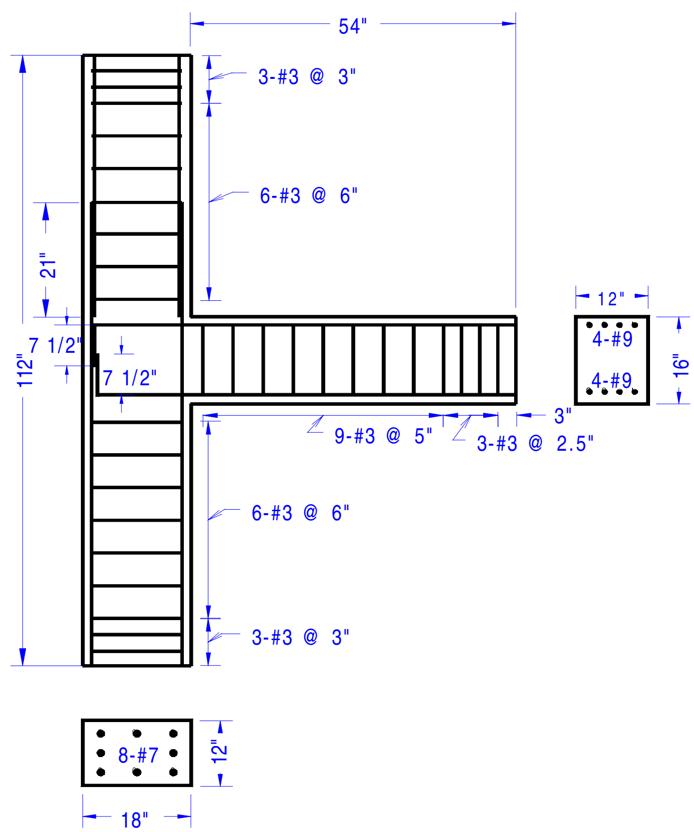

Fig. 2.1 Specimen dimensions and reinforcement details

The beam is 12 in. (30.5 cm) wide and 16 in. (40.6 cm) deep. It is symmetrically reinforced with 4-#9 bars for both the positive and negative reinforcement; the steel ratio is 2.47% at both top and bottom. Each longitudinal bar has a 7.5 in. (19.1 cm) hook bent at 90°. The bottom beam reinforcement is bent up into a hook at the joint, and the top reinforcement is bent down into a hook at the joint. The hooks overlap approximately 2 in. (5.1 cm) and are tied together, one inside the other as shown in Fig. 2.1. The transverse reinforcement is a #3 bar closed stirrup with 140° bend and 2.5 in. (6.35 cm) extension on both ends as shown in Fig. 2.2. The stirrups are spaced at 5 in. (12.7 cm) along the beam except within 8 in. (20.3 cm) of the beam end, where the spacing is reduced by half to 2.5 in. (6.35 cm). The closer spacing is intended to give adequate strength at the location where the force is applied during the test.

It should be noted that the original half-scale calculations required a reinforcement ratio ρ=0.76% in the top and ρ=0.48% in the bottom. The decision to increase the beam longitudinal reinforcement was based on our objective to study joint shear failure at high drift levels and not beam flexural degradation. The 2.47% of longitudinal steel present in both the top and bottom of the beam meant that the design joint core shear forces developed would be relatively high.

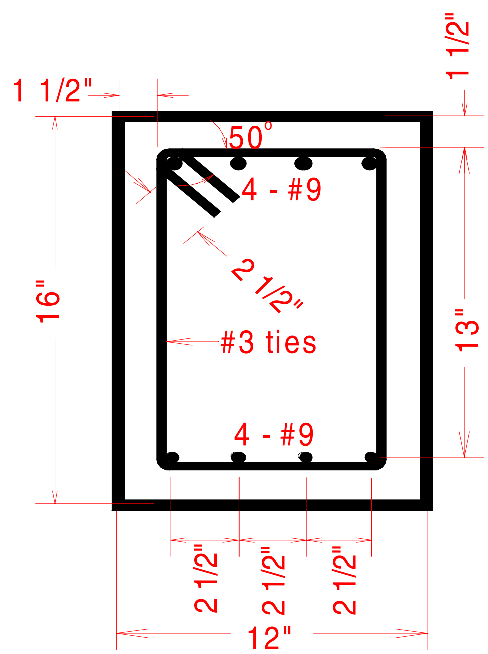

Fig. 2.2 Beam cross section

The column is 12 in. (30.5 cm) wide and 18 in. (45.7 cm) deep. It is reinforced with 8-#7 bars evenly distributed around the perimeter of the column, thus having a steel ratio of 2.54%.

The longitudinal reinforcement in the bottom column extends continuously up through the joint and 21 in. (53.3 cm) into the top column, as shown in Fig. 2.1. The top column longitudinal reinforcement is spliced over the 21 in. (53.3 cm) length and extends to the upper end of the column, or a distance $24d_b$, which is insufficient by current standards. The transverse reinforcement in the column consists of #3 bar closed stirrups with 140° bends and 2.5 in. (6.35 cm) extensions on both ends; this is shown in Fig. 2.3. The stirrups are spaced at 6 in. (15.2 cm) along the height of the column, except within the joint region where there is no transverse reinforcement. The spacing is decreased to 3 in. (7.6 cm) at the upper and lower ends of the column, where the column was supported during the test.

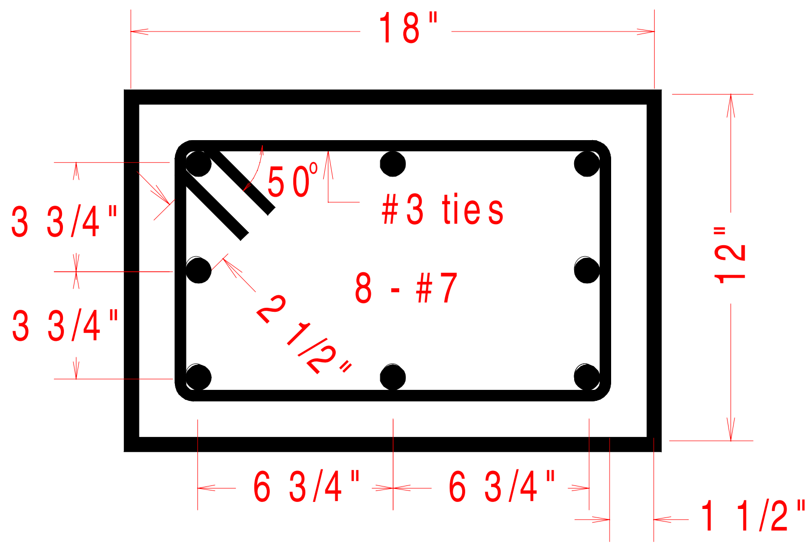

Fig. 2.3 Column cross section

The specimens were constructed and cast in place, one at a time, over a period of several weeks. Each reinforcement cage was securely tied together and placed upon metal chairs in the wooden forms to hold it in place as the concrete was poured. A high-frequency vibrator was used to consolidate the concrete and reduce honeycombing, especially in the joint region. An accelerated, 24-hour heat cure was used on each specimen; thus each was stripped from the form the day after it was poured.

3 Test Setup

3.1 INSTRUMENTATION

3.1.1 Strain Gages

Strain gages were placed on both the longitudinal and transverse reinforcement at selected locations within the concrete beam-column joints. The gages were attached and wired to the steel cage and precautions were taken to protect them while the concrete was poured. The locations of the strain gages were determined based on where yielding and hinging was expected to occur in the specimen during testing. Four gages were placed on longitudinal beam reinforcement at the face of the joint. Four gages were placed on longitudinal column reinforcement at both the top and bottom faces of the joint. Several gages were also attached at the end of the lap splice and on two stirrups in the lap splice region, as shown in Fig. 3.1.

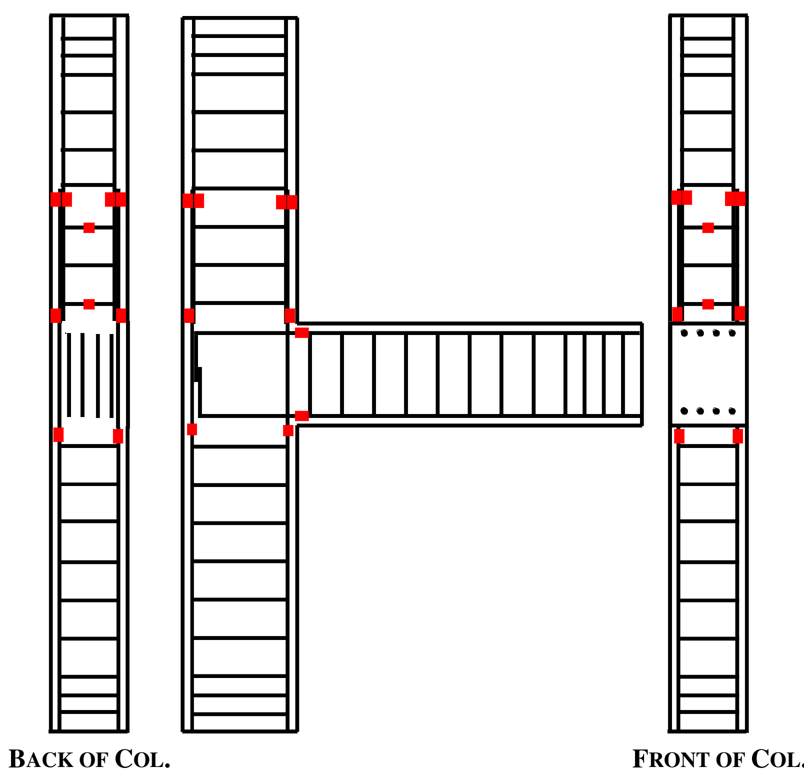

Fig. 3.1 Strain gage locations

3.1.2 LVDT

A configuration of 11 linear variable differential transducers (LVDTs) was mounted unobtrusively on the column at the face of the joint and in the lap splice region to measure movement in these areas. The data from these LVDTs, shown in Fig. 3.2, were used to calculate shear strain.

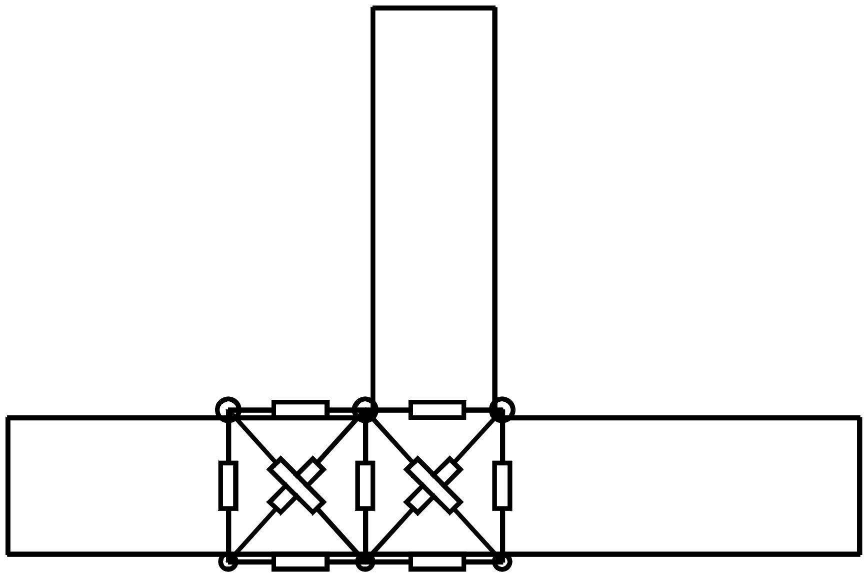

Fig. 3.2 LVDT configuration

3.1.3 Displacement Transducers

Displacement transducers were attached to each specimen to measure curvature in the beam, rotation in the joint, deflection at the end of the beam, and rigid body movement of the specimen, as shown in Fig. 3.3.

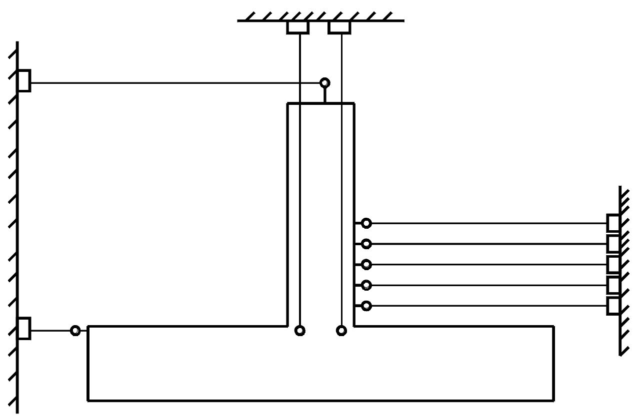

Fig. 3.3 Displacement transducer locations

3.2 LOADING APPARATUS

A schematic of the loading apparatus is shown in Fig. 3.4. The column was mounted horizontally with pinned supports at both ends. The axial load was applied using a small hydraulic cylinder and transferred to the column through four threaded rods. These rods were instrumented with strain gages that allowed measurement of the axial load. The lateral load was applied at the end of the beam through a loading collar, as shown below. A load cell situated between the hydraulic actuator and the loading collar measured the quasi-static cyclic load applied to the beam. The actuator was pinned at the end to allow rotation during the test. This loading device was manually operated.

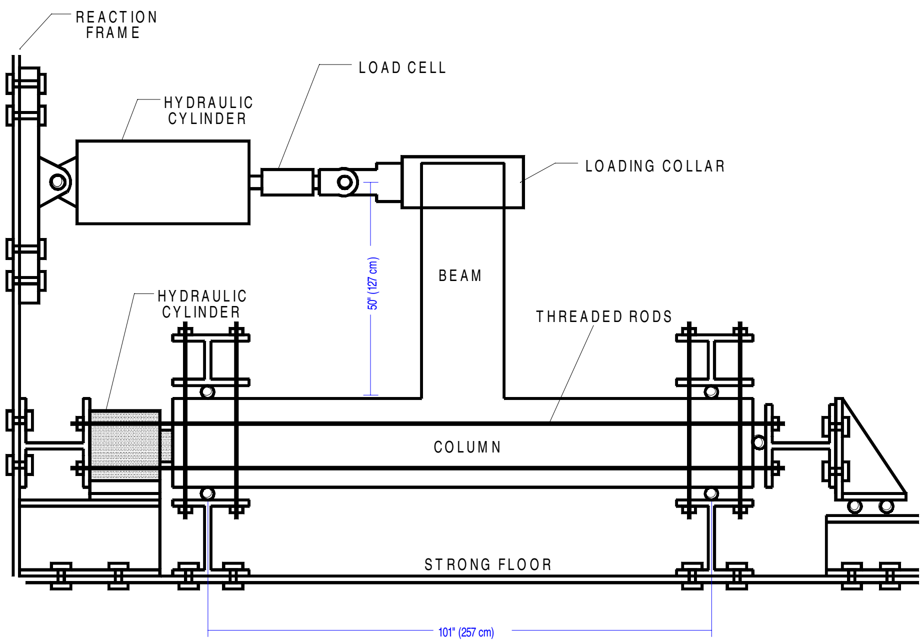

Fig. 3.4 Test setup

3.3 TEST PROCEDURE

First, the axial load was applied to the column portion of the specimen. An axial compressive load equal to $0.1f'_cA_g$ was applied to two of the specimens, Test 2 and Test 6. The other two specimens, Test 4 and Test 5, received an axial compressive load equal to $0.25f'_cA_g$. The axial load was set to the calculated initial value and then left to change at will as the beam was subjected to lateral reversals.

The lateral load was applied cyclically through the loading collar, in a quasi-static fashion, at the end of the beam, as shown in Fig. 3.4. The first portion of the test was loadcontrolled wherein the lateral load was increased in 5 kip (22.2 kN) increments. At every load step, three cycles were performed. The average cycle took 40 seconds to complete. Each cycle contained a push and pull segment. After the first yielding of the longitudinal reinforcement, the testing was carried out using displacement-control. Three cycles were performed at each displacement step, and the displacement was increased as a fraction of the initial yield displacement. The test continued until the lateral load dropped below approximately 50% of the peak value. The loading procedure for Test 4 is shown in Fig. 3.5 and is typical of all four tests.

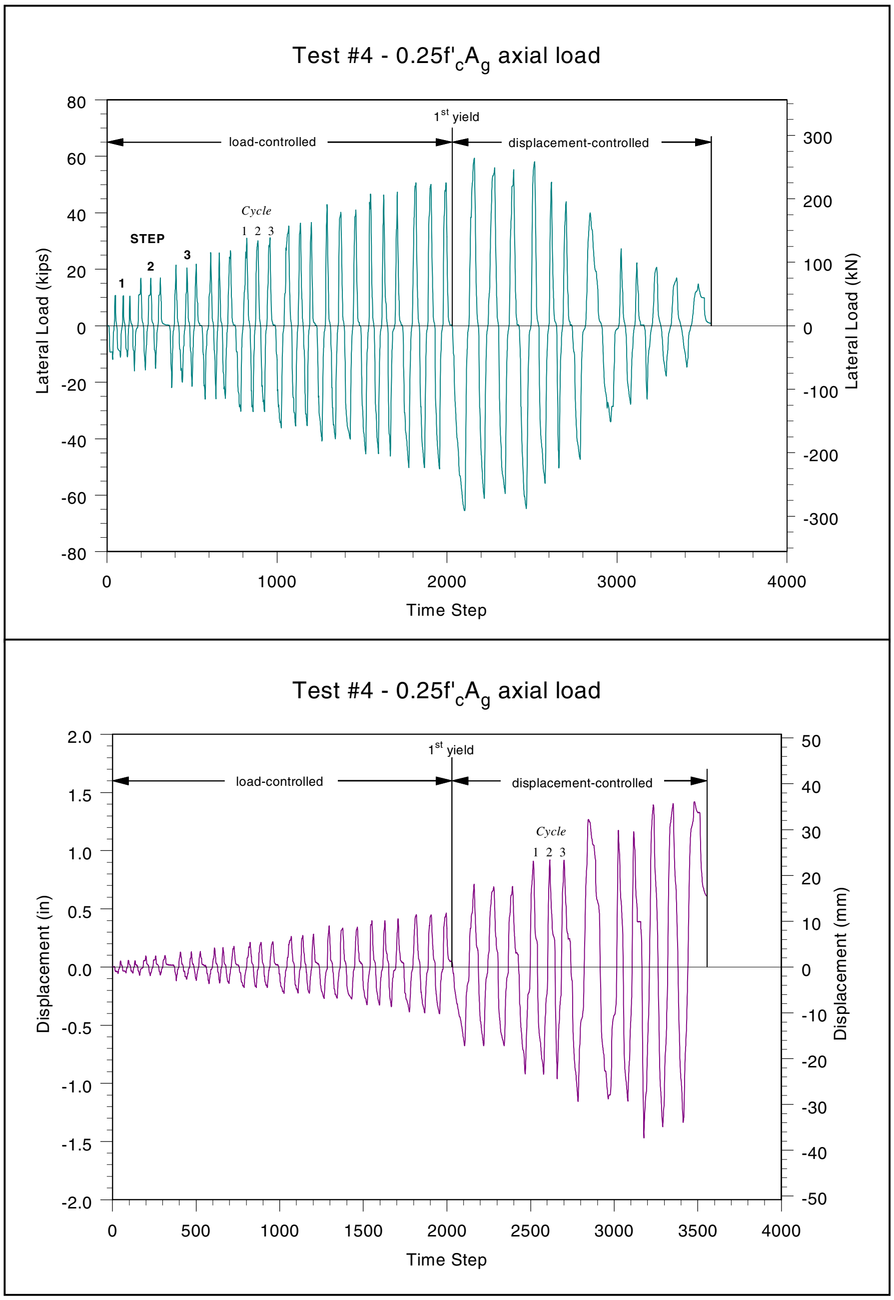

Fig. 3.5 Typical loading pattern

4 Experimental Results and Discussion

Following the testing procedure described in the previous section, four as-is reinforced concrete joints were tested. The experimental results of each beam-column joint specimen are discussed in this section. The results presented in this report include

- load-drift hysteresis loops
- description of damage
- peak load, peak displacement, bilinear displacement ductility
- nominal joint shear stress vs. shear strain diagrams
- axial load behavior
- energy dissipation

Two different column axial load levels were used in the testing. Two specimens (Test #2 and Test #6) were tested with an axial load equal to 10% of f'_cA_g, and two (Test #4 and Test #5) were tested with an axial load equal to 25% of f'_cA_g. The specimens in the different load levels are discussed separately and then compared at the end of this section.

4.1 TESTS WITH 10% AXIAL LOAD

4.1.1 Test #2

The load versus drift curve is shown in Fig. 4.1. The load step number is shown next to the first cycle of that step. The first yielding occurred in a bottom, longitudinal beam bar in load step four. The lateral load at yielding was 20.9 kips (93 kN) at a lateral displacement of 0.31 in. (7.8 mm). Only hairline cracking was apparent at this point during the test. Measurable flexural cracks in the beam and shear cracks in the joint appeared during the seventh load step corresponding to a lateral load of approximately 40 kips (178 kN). The subsequent loading steps produced only slight increase in crack widths in the beam. However, the shear cracking in the joint rapidly increased to a maximum average crack width of 0.18 in. (4.5 mm) by the end of the test. Shear cracks had also spread to the column where they extended up along the longitudinal column bars. Fig. 4.2 shows the damage the joint incurred from the lateral loading. The joint ultimately failed at a displacement of 1.94 in. (4.9 cm) corresponding to a drift of 2.95%. The displacement ductility of the joint was determined to be μ=2.8 through a bilinear model approximation. The peak lateral load sustained by the specimen was 60.1 kips (267 kN). By the end of the test, the load had dropped to 30.1 kips (134 kN) which is 53% of the peak load.

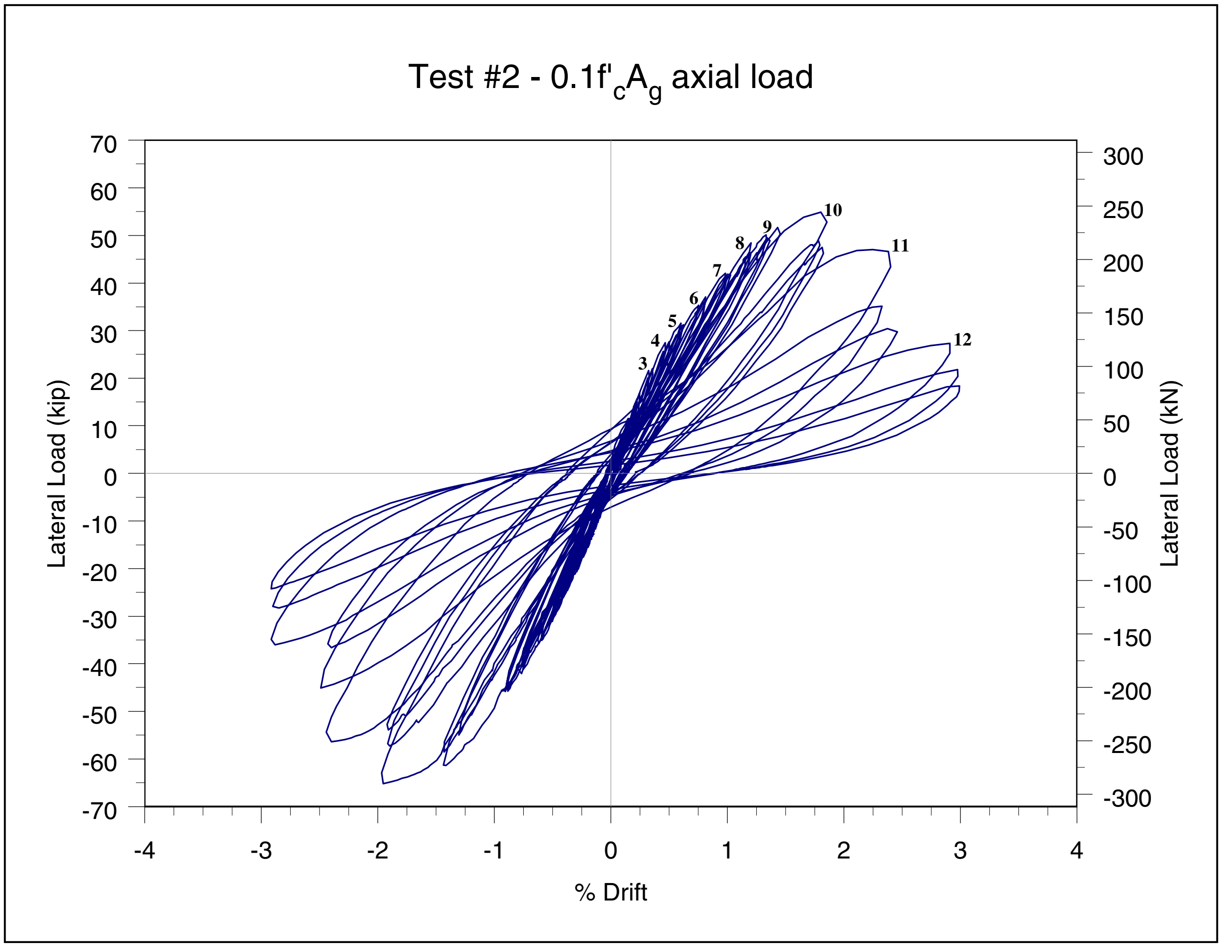

Note: **10** = first cycle of load step number 10

Fig. 4.1 Test #2 load-drift curve

Ultimate failure of the beam-column specimen is attributed to the development of the limiting joint shear capacity. The joint shear behavior can be seen in Fig. 4.3. This diagram shows nominal joint shear stress versus joint shear strain. The nominal joint shear stress is the average stress in the joint normalized by $\sqrt{f'_c}$, which is also referred to as the joint strength coefficient, γ, in this report. The specimen in test #2 reached a maximum stress of 992 psi (6.8

MPa) or γ=12.1 (psi) [γ=1.00 (MPa)]. This value far exceeds the value of γ=6 (psi) [γ=0.50 (MPa)] prescribed in FEMA 273 for this type of joint and just reaches the value of γ=12 (psi) [γ=1.00 (MPa)] for a new, Type II joint by ACI 352 (1991) standards, as shown in Fig. 4.3.

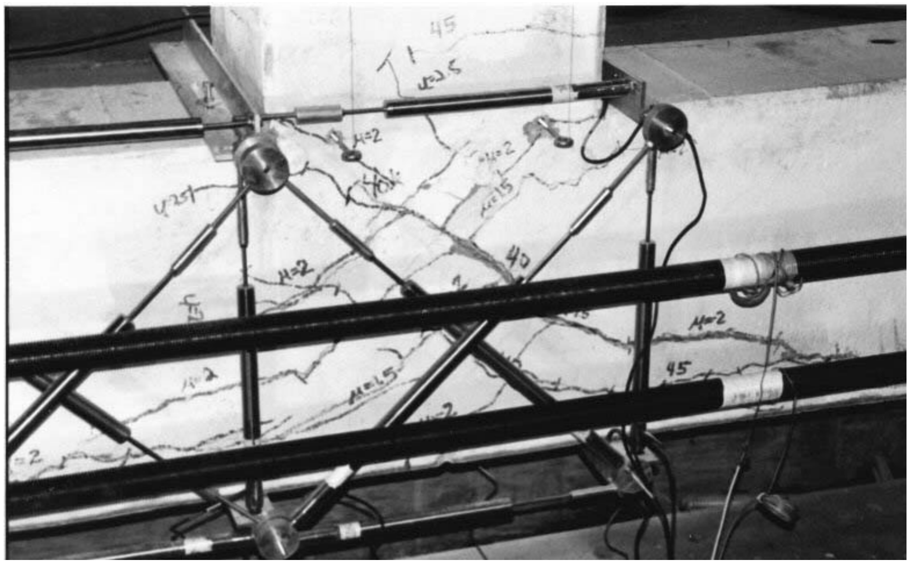

Fig. 4.2 Damage to Test #2 specimen

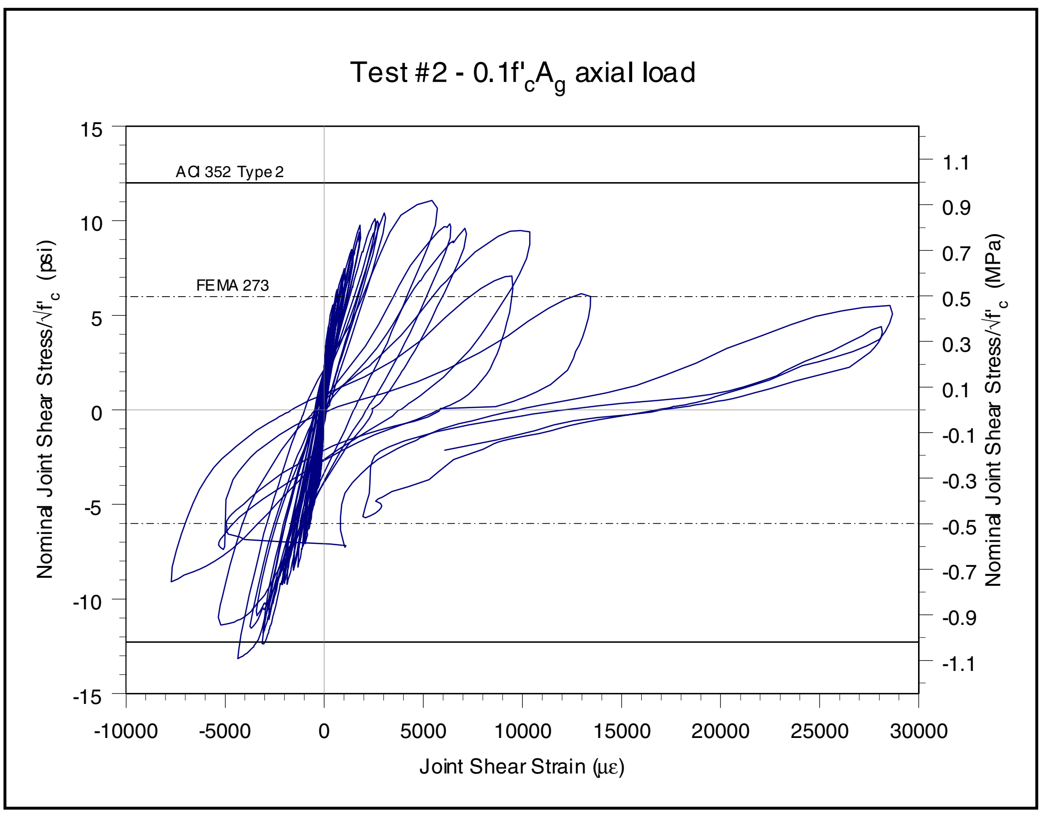

Fig. 4.3 Test #2 joint shear behavior

The maximum nominal joint shear stress occurred at a joint shear strain equal to 0.0045. The response of the column to the cyclic loading is represented by the plot of axial column load shown in Fig. 4.4. The axial compressive load in the column was originally set at 155 kips (689 kN) corresponding to $0.1f'_cAg$. Fig. 4.4 shows how the axial load fluctuated as the specimen was subjected to the various loading cycles. This fluctuation is a result of the testing setup, which used threaded steel rods to transfer the axial load to the column. As the beam was pushed, the rods were put into additional tension, and as the beam was pulled the tension was somewhat released. Although in an actual building the compressive load in a column would vary differently, the fluctuations evident in this test are considered reasonable.

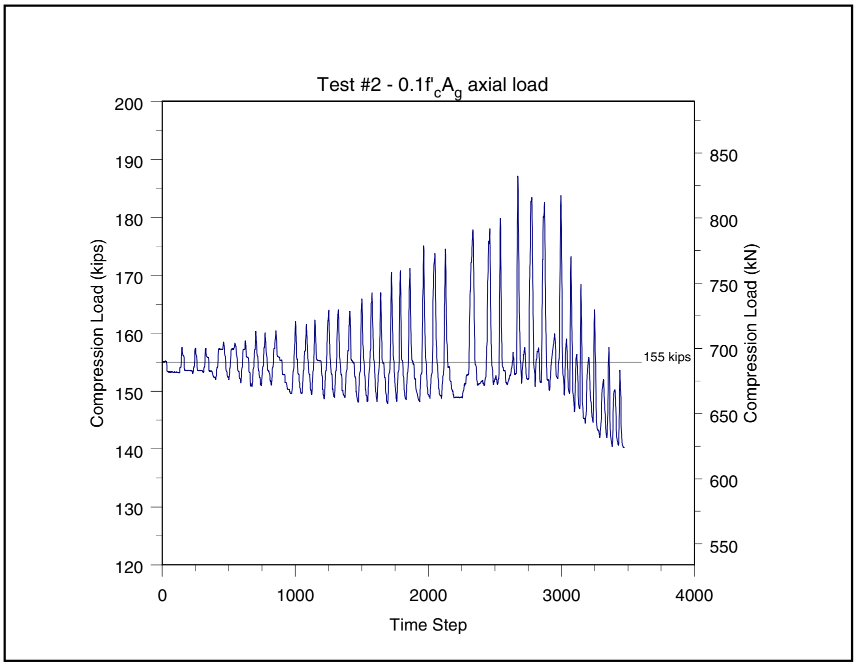

Fig. 4.4 Test #2 column axial load

The relationship between the column axial load and drift, and the column axial load and imposed lateral load are shown in Fig. 4.5(a) and Fig. 4.5(b), respectively. These plots illustrate that the overall axial load in the column deteriorated during the test. At the conclusion of the test, the column carried 140 kips (623 kN) of compressive load. This is a 10% drop from the axial load that was initially applied. This drop in the axial load can not be taken to mean that the axial capacity of the column was reduced, but rather it reflects the loss of stiffness due to progressive cracking in the joint and column at higher drift levels.

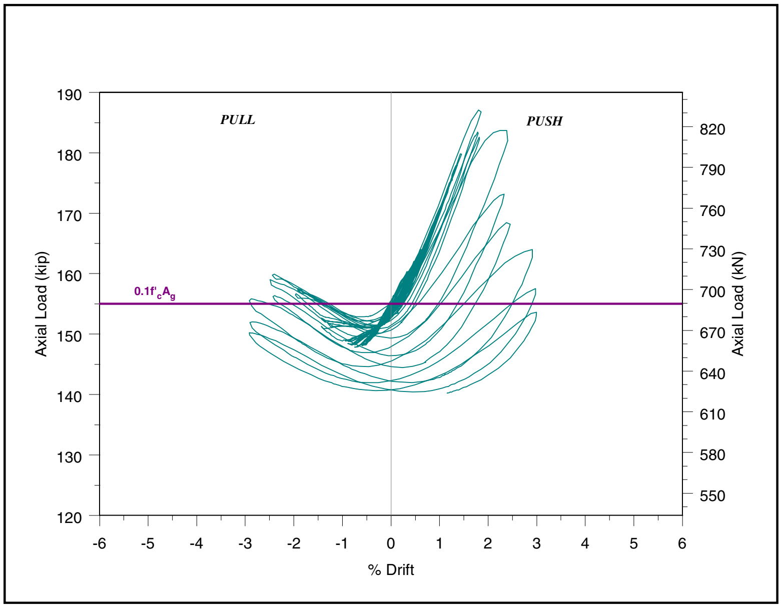

(a)

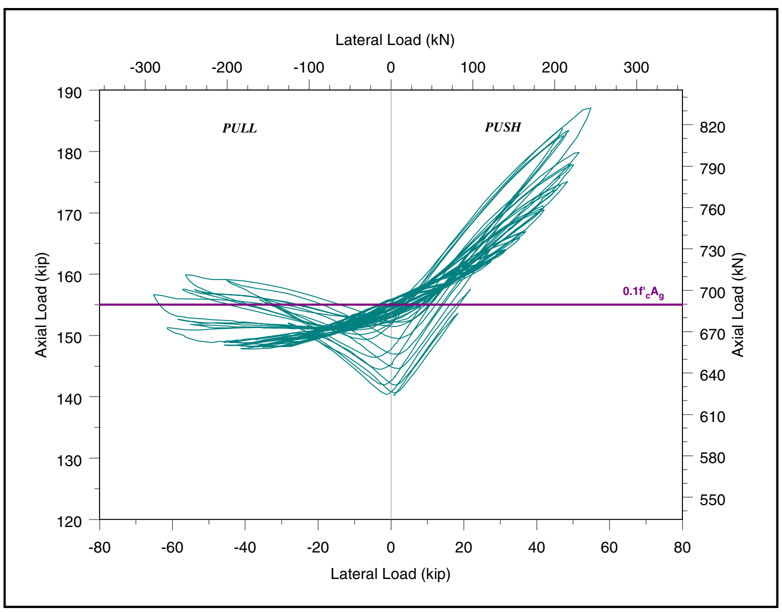

(b)

Fig. 4.5 Test #2 axial load deterioration

The amount of cumulative energy dissipated in the joint is shown in Fig. 4.6. Only a small amount of energy was absorbed during the first several loading steps. As the beam-column specimen was damaged due to the cyclic loading at higher drift levels, the energy absorption rapidly increased. This occurred at approximately the ninth loading step or a drift of 1.3%, as shown in Fig 4.6. By the end of the test the joint had dissipated a cumulative 461 k-in. (52 kJ) of energy. The joint had dissipated 14.5% of the total energy at 1% drift, 44.9% of the energy at 2% drift, and 100% of the energy at 2.95% drift.

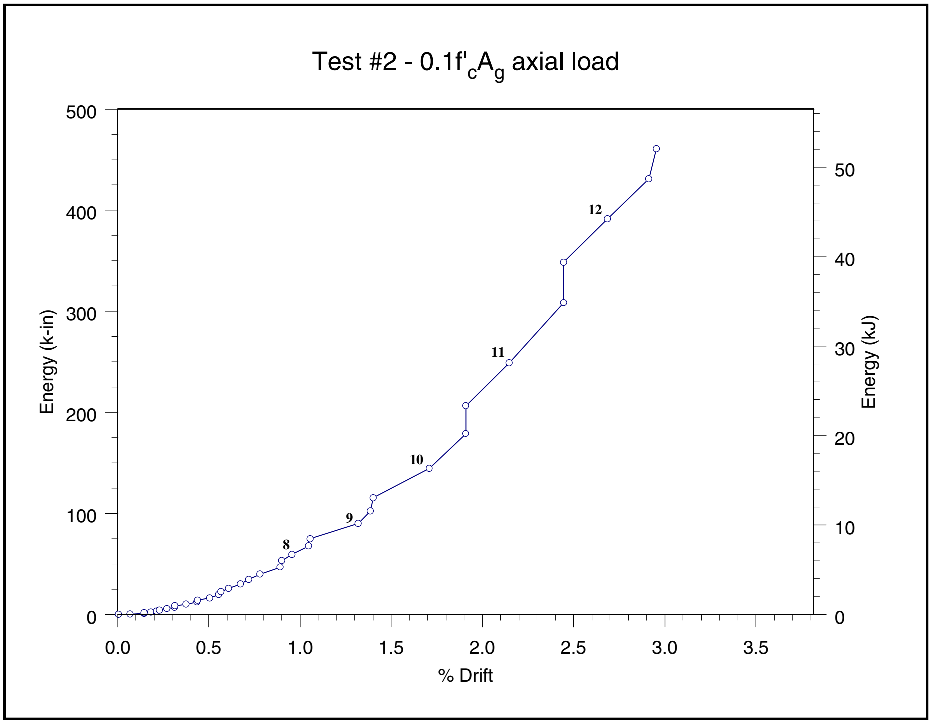

Note: **10** = first cycle of load step number 10

Fig. 4.6 Energy dissipation in Test #2

4.1.2 Test #6

The load-drift hysteresis diagram for the beam-column joint in Test #4 is shown in Fig. 4.7. At 29.0 kips (129 kN) of lateral load, the first longitudinal reinforcement yielded in the beam. Yielding occurred during the fifth load step in a bottom beam bar at a lateral displacement of 0.38 in. (9.7 mm). Hairline flexural cracks in the beam and shear cracks in the joint formed during this loading cycle as well. A somewhat larger crack was also apparent at the interface between the beam and the column. The sixth loading step, corresponding to a lateral load of approximately 35 kips (156 kN), produced measurable shear cracks in the joint and beam, which increased as the cyclic loading continued. The final maximum crack width in the beam was 0.01 in. (0.25 mm). The joint received much more damage with an average diagonal shear crack width of 0.79 in. (20 mm). These diagonal cracks had spread to the column creating a triangular cracked section that spalled off the back of the column by the end of the test. Fig. 4.8 shows the damage described above. The joint specimen reached a displacement of 2.35 in. (6.0 cm) or 3.57% drift at ultimate failure. The peak lateral load sustained by the specimen was 59 kips (262 kN). The load had dropped 51% from the peak to 29 kips (129 kN) by the end of the test. The bilinear model displacement ductility of the joint is μ=2.6.

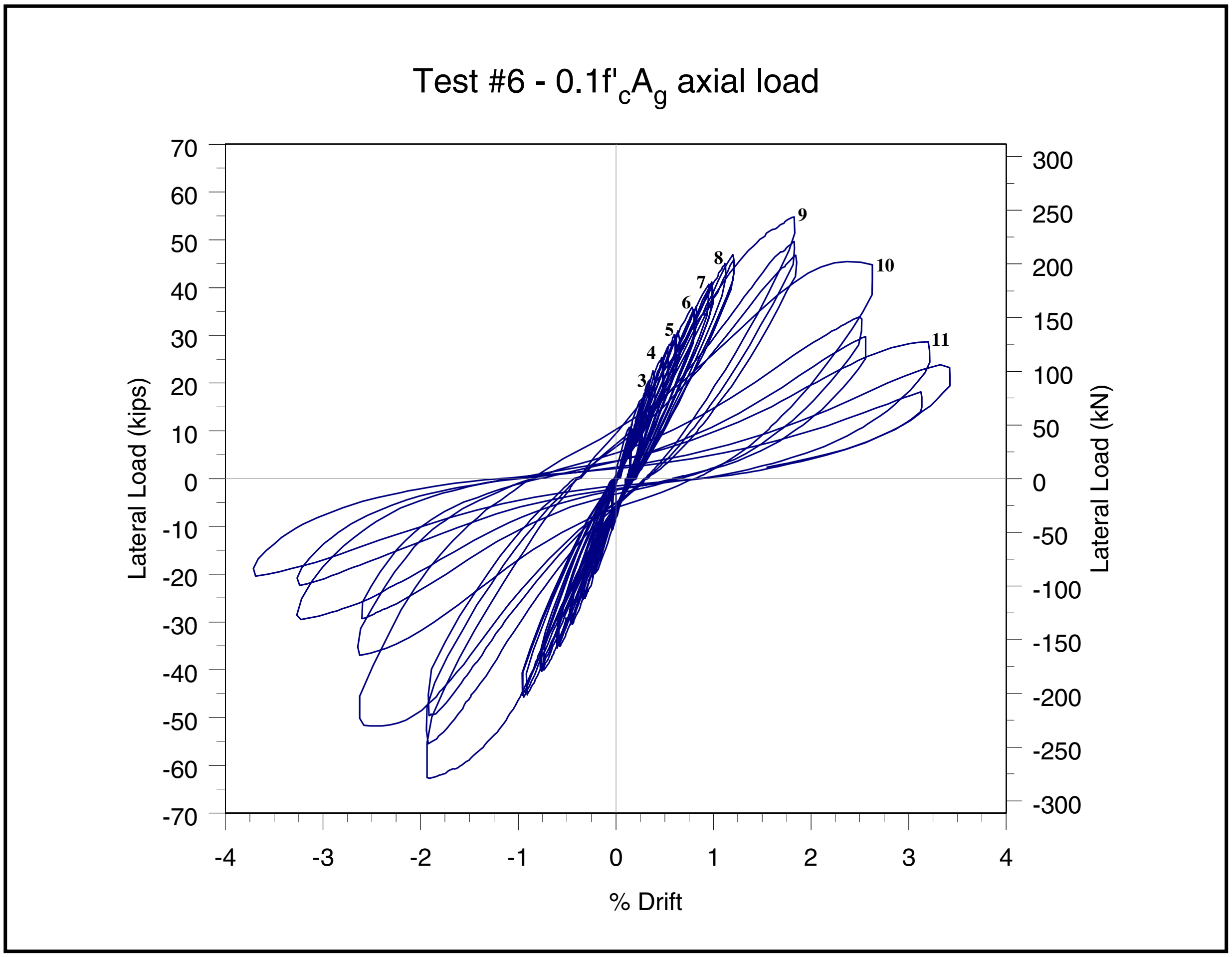

Note: **10** = first cycle of load step number 10

Fig. 4.7 Test #6 load-drift curve

Ultimate failure of the beam-column specimen is attributed to the development of the limiting joint shear capacity. Fig. 4.9 illustrates the joint shear behavior. The maximum joint shear stress reached in test #6 was 970 psi (6.7 MPa) which normalized by $\sqrt{f'_c}$ is γ=12.7 psi [γ=1.05 (MPa)]. As seen in the diagram, this stress level exceeds that prescribed in FEMA 273 and ACI 352. The maximum nominal joint shear stress occurred at a joint shear strain of 0.0035.

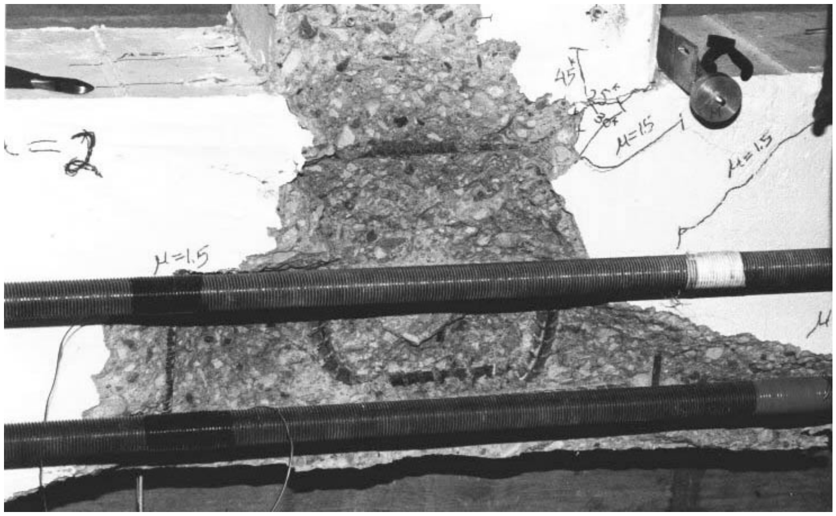

Fig. 4.8 Damage to Test #6 specimen

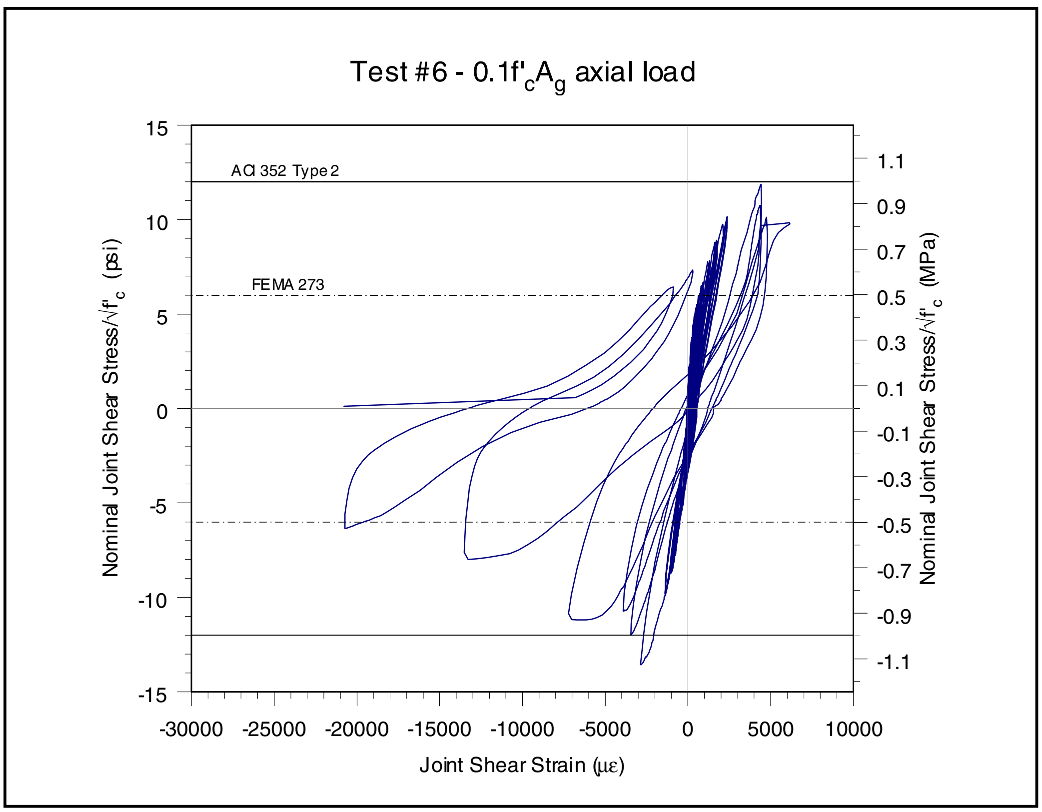

Fig. 4.9 Test #6 joint shear behavior

The compression load in the column was initially set at $0.1f'_cA_g$ which is 132 kips (587 kN). The behavior of the column axial load is shown in Fig. 4.10 and 4.11. The fluctuation during the pushing and pulling load pattern is similar to that which occurred in Test #2. The plots shown in Fig. 4.10(a) and (b) show the reduction of the column axial load. The compressive load dropped 24% from the original value to 100 kips (445 kN) by the end of the test.

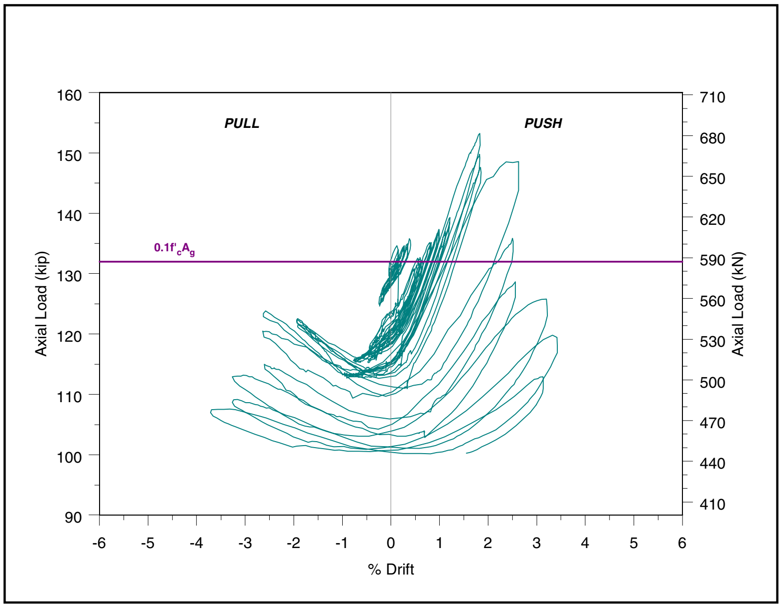

(a)

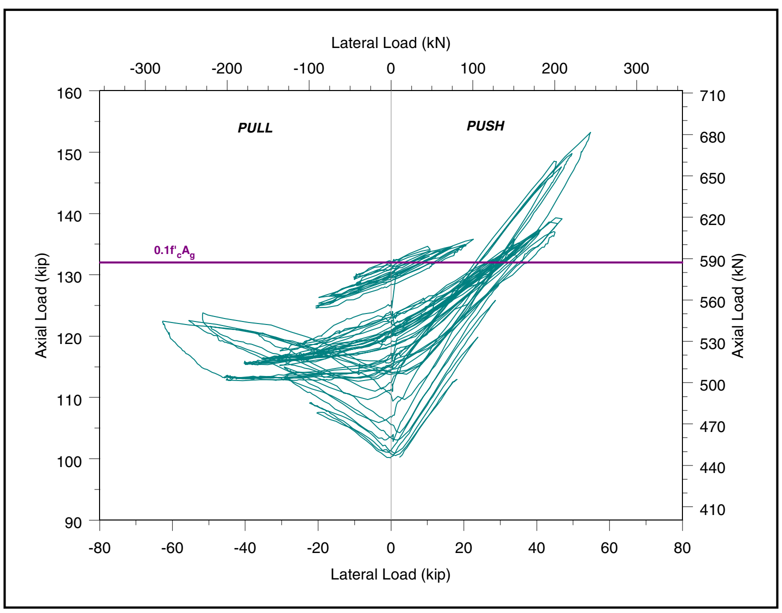

(b)

Fig. 4.10 Test #6 axial load deterioration

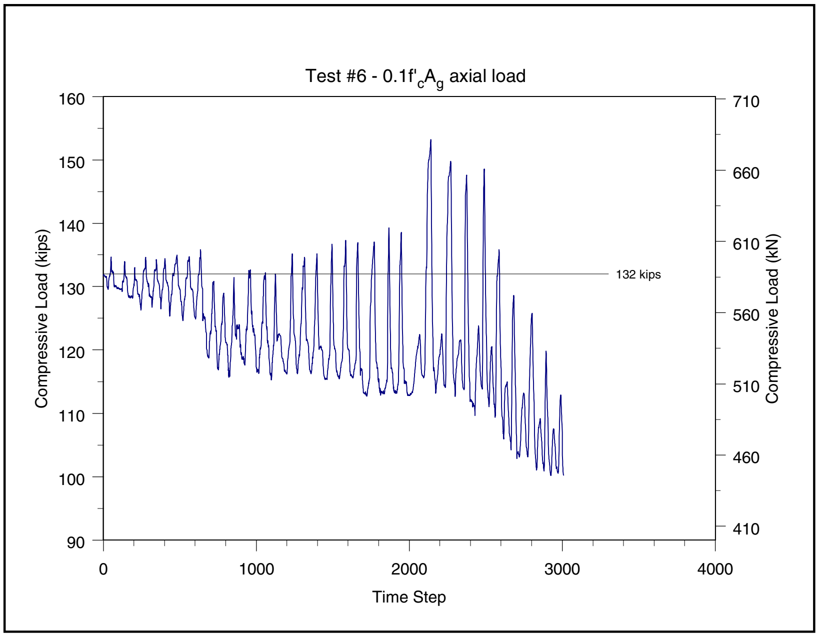

Fig. 4.11 Test #6 column axial load

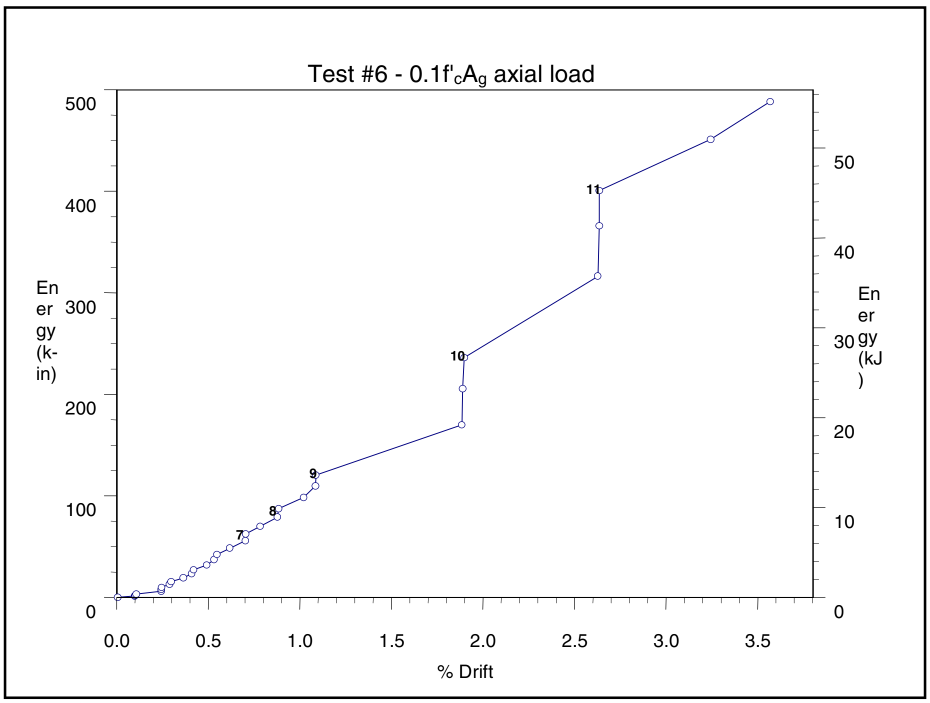

Note: **10** = first cycle of load step number 10

Fig. 4.12 Energy dissipation in Test #6

The energy absorbed during the cyclic loading of the specimen in Test #6 is shown in Fig. 4.12. As in Test #2, very little energy was dissipated in the initial loading cycles. The last four loading steps of the test show accelerated energy absorption starting at the ninth load step or a drift of 1.1%. The joint ultimately dissipated a total of 488 k-in. (55 kJ) of energy during the test. At 1% drift the joint had dissipated 20.1% of the total energy, at 2% drift the joint had dissipated 48.6%, and at 3% drift the joint had dissipated 92.0% of the total dissipated energy.

4.2 TESTS WITH 25% AXIAL LOAD

4.2.1 Test #4

A picture of the joint at the end of the test is shown in Fig. 4.13. The load-drift hysteresis diagram for the beam-column joint in Test #4 is shown in Fig. 4.14. Initial hairline cracking in the beam and joint started in the second load step. However, these cracks did not start widening until load step 7. Strain gage readings indicate that the first longitudinal reinforcement yielded in the first cycle of load step 9. Yielding occurred at a lateral load of 50.7 kips (226 kN) in a top beam bar with a yield displacement of 0.45 in. (11.4 mm), which is 30% greater than the average of the $0.1f'_cA_g$ specimens. At this point in the test, measurable cracks had already formed in the beam and joint, but major cracking did not occur until load step 10 following yielding which corresponded to a lateral load of 60 kips (267 kN). The joint received the most amount of damage with an average diagonal shear crack width of 0.35 in. (9 mm). Spalling of the concrete occurred at the end of the test. The diagonal shear cracks in the joint spread to the column in the eleventh load step. The average maximum column crack width at the end of the test was 0.20 in. (5 mm). The joint specimen reached a maximum displacement of 1.45 in. (3.7 cm) and 2.2% drift at ultimate failure. The peak lateral load sustained by the specimen was 62 kips (276 kN). The load had dropped to 23 kips (102 kN) by the end of the test, which is 37% of the peak load. The bilinear model displacement ductility of the joint is μ=1.8.

Fig. 4.13 Damage to Test #4 specimen

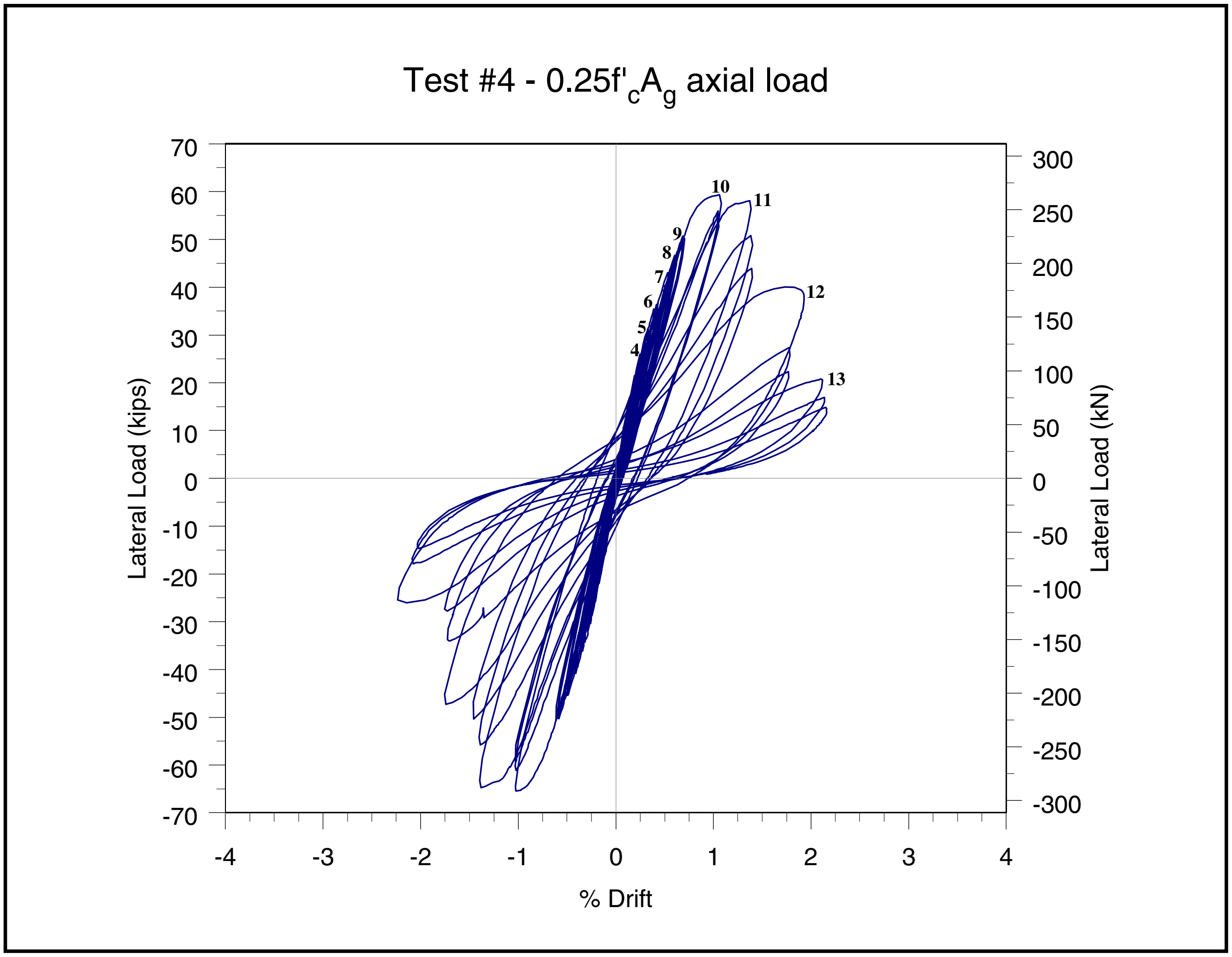

Note: **10** = first cycle of load step number 10

Fig. 4.14 Test #4 load-drift curve

Ultimate failure of the beam-column specimen in test #4 is attributed to development of the limiting joint shear capacity. The maximum joint shear stress was 1031 psi (7.1 MPa) which corresponds to a γ=13.4 (psi) [γ=1.11 (MPa)]. Fig. 4.15 depicts the joint shear behavior. As seen in the diagram, the joint reached a stress level beyond that prescribed in FEMA 273 and ACI 352. The maximum nominal joint shear stress occurred at a joint shear strain of 0.035.

Test #4 was the first specimen to be tested with a 25% axial compressive load in the column. The initial column load was set at 310 kips (1380 kN). The behavior of the axial load during the cyclic, lateral loading is shown in Fig. 4.16. The fluctuation seen in the diagram is a result of the test setup; extensive cracking in the joint and column resulted in loss of stiffness at high drift levels. The column load reduction from the full $0.25f'_cA_g$ axial load is due to the closure of cracks that opened in the push cycle and closed in the pull cycle. This reduction is shown in Fig. 4.17(a) and (b). By the end of the test, the compressive load had dropped 17% from the original value to 257 kips (1143 kN).

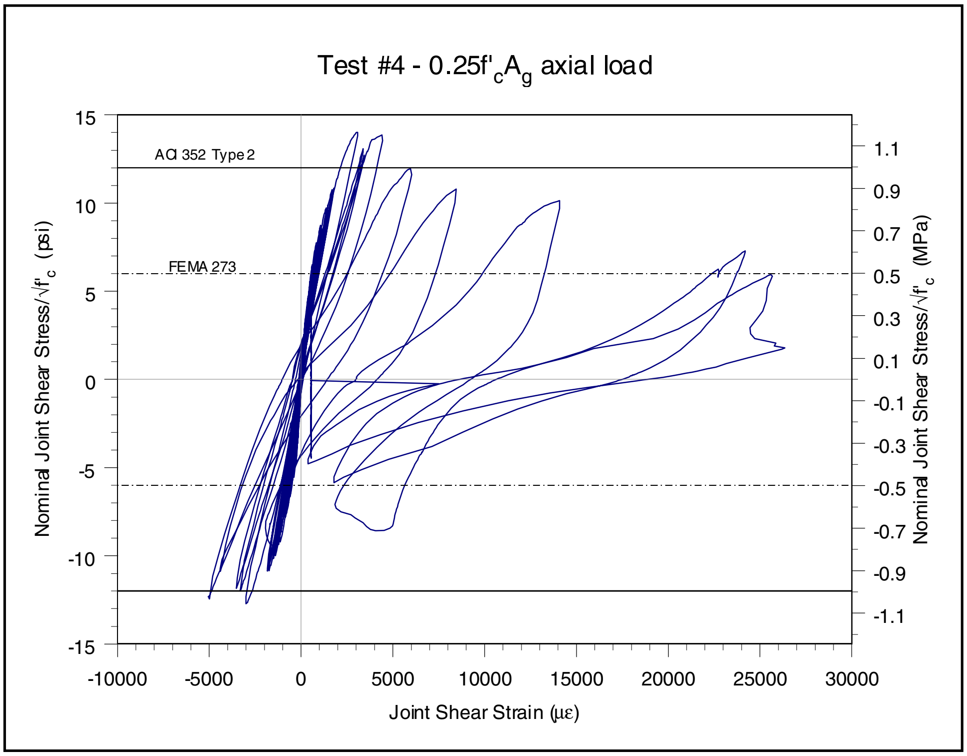

Fig. 4.15 Test #4 joint shear behavior

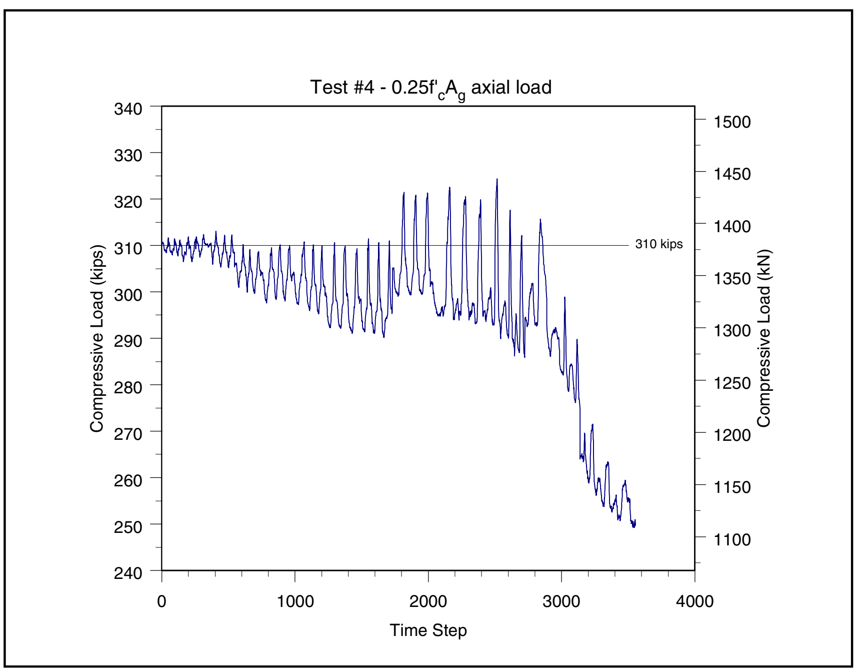

Fig. 4.16 Test #4 column axial load

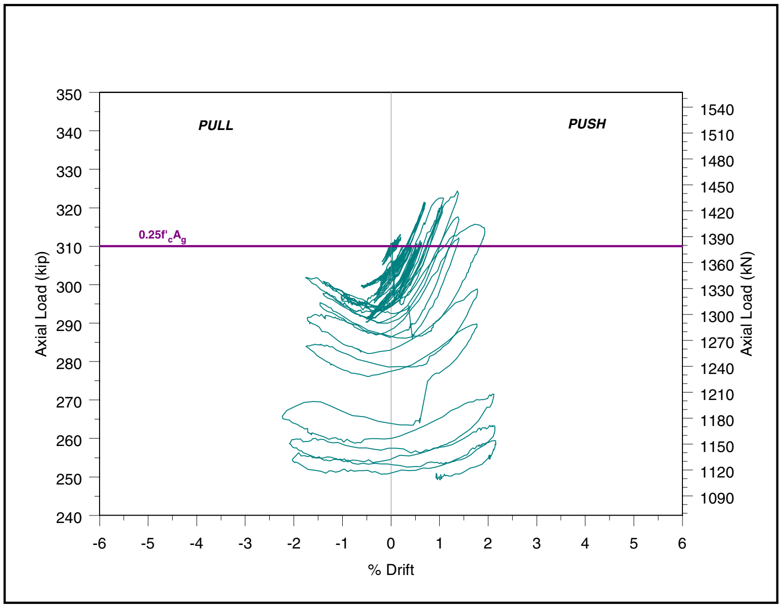

(a)

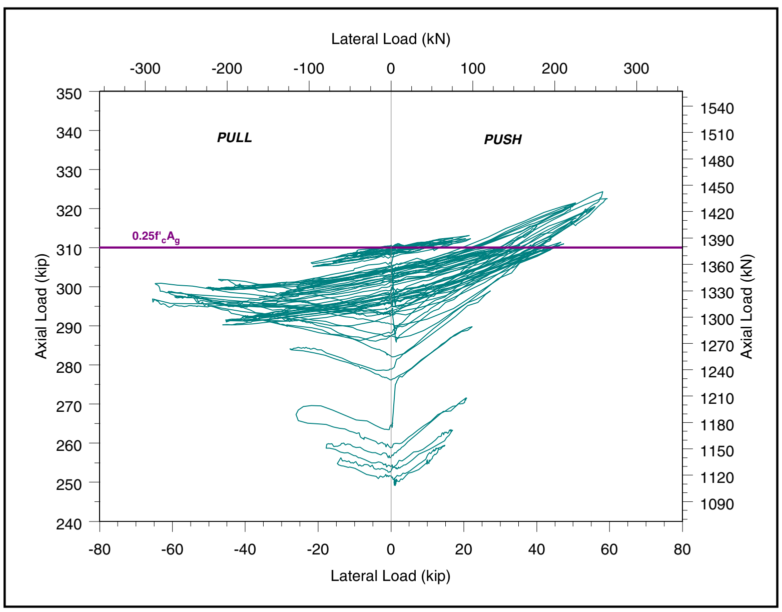

(b)

Fig. 4.17 Test #4 axial load deterioration

The energy absorbed during the cyclic loading of the beam-column specimen is shown in Fig. 4.18. Similar to the previous two tests, slow energy absorption characterized the majority of the test. Accelerated absorption occurred in the later stages of loading from step 10 to step 13, as shown on the diagram, starting at the tenth step or a drift of 0.9%. The joint ultimately dissipated a total of 370 k-in. (42 kJ) of energy during the test. It should be noted that at 1% and

2% drift the joint had dissipated 26.8% and 90.5% of the energy, respectively. The specimen never reached 3% drift.

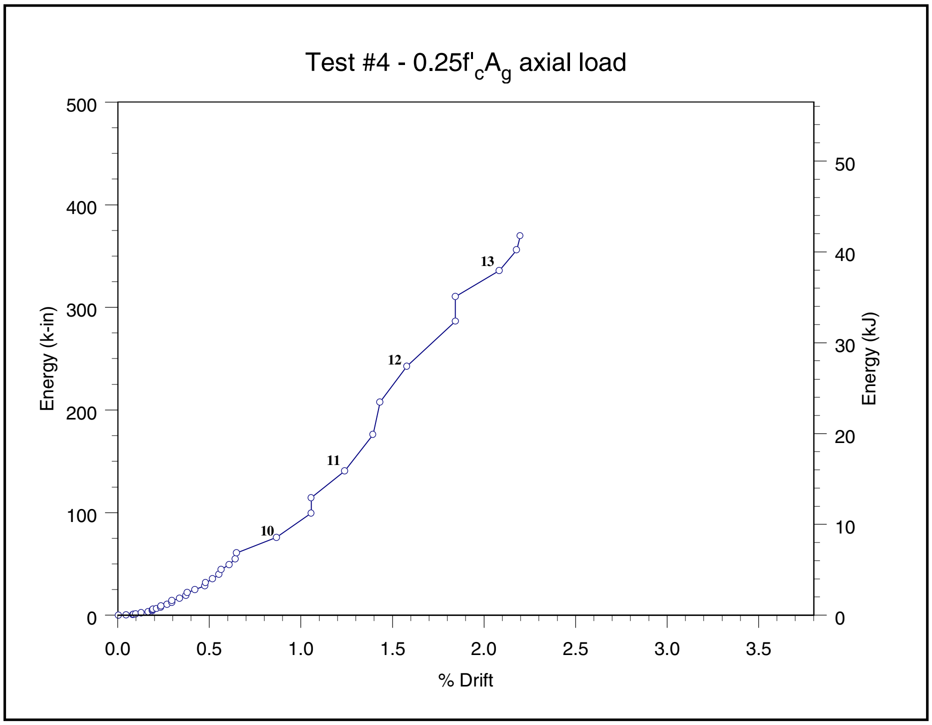

Note: **10** = first cycle of load step number 10

Fig. 4.18 Energy dissipation in Test #4

4.2.2 Test #5

The load versus drift hysteretic curve for the beam-column joint in Test #5 is shown in Fig. 4.19. The first yielding in the specimen occurred in a top, longitudinal beam bar in the second cycle of load step 9. The lateral load corresponding to this yield point is 52.0 kips (231 kN). The yield displacement was 0.70 in. (17.8 mm), which is on average 100% greater than the $0.1f'_cA_g$ specimens. Cracks 0.006 in. (0.15 mm) in width were already present in both the beam and joint at this point in the test. A crack was also apparent at the interface between the beam and the column. The load cycles following yield showed a rapid increase in crack width in the joint, while the beam and interface cracks did not show much increase. The final maximum crack width in the beam was 0.07 in. (1.7 mm). The joint, on the other hand, had an average diagonal shear crack width of 0.33 in. (8.5 mm) by the end of the test. These diagonal cracks had entered the column causing a large vertical crack and major spalling on the back of the joint. With so much concrete absent in the joint region, the longitudinal column reinforcement was forced to carry a substantial amount of the compressive axial load. This resulted in column bar buckling. Fig. 4.20 shows the described damage to the joint specimen where buckling of the longitudinal column bars is apparent. The joint ultimately failed at a displacement of 1.90 in. (4.8 cm) corresponding to a drift of 2.90%. The peak lateral load sustained by the specimen was 60 kips (267 kN). By the end of the test, the lateral load had dropped 63% from the peak load to 22 kips (98 kN). The bilinear model displacement ductility of the joint is μ=1.4.

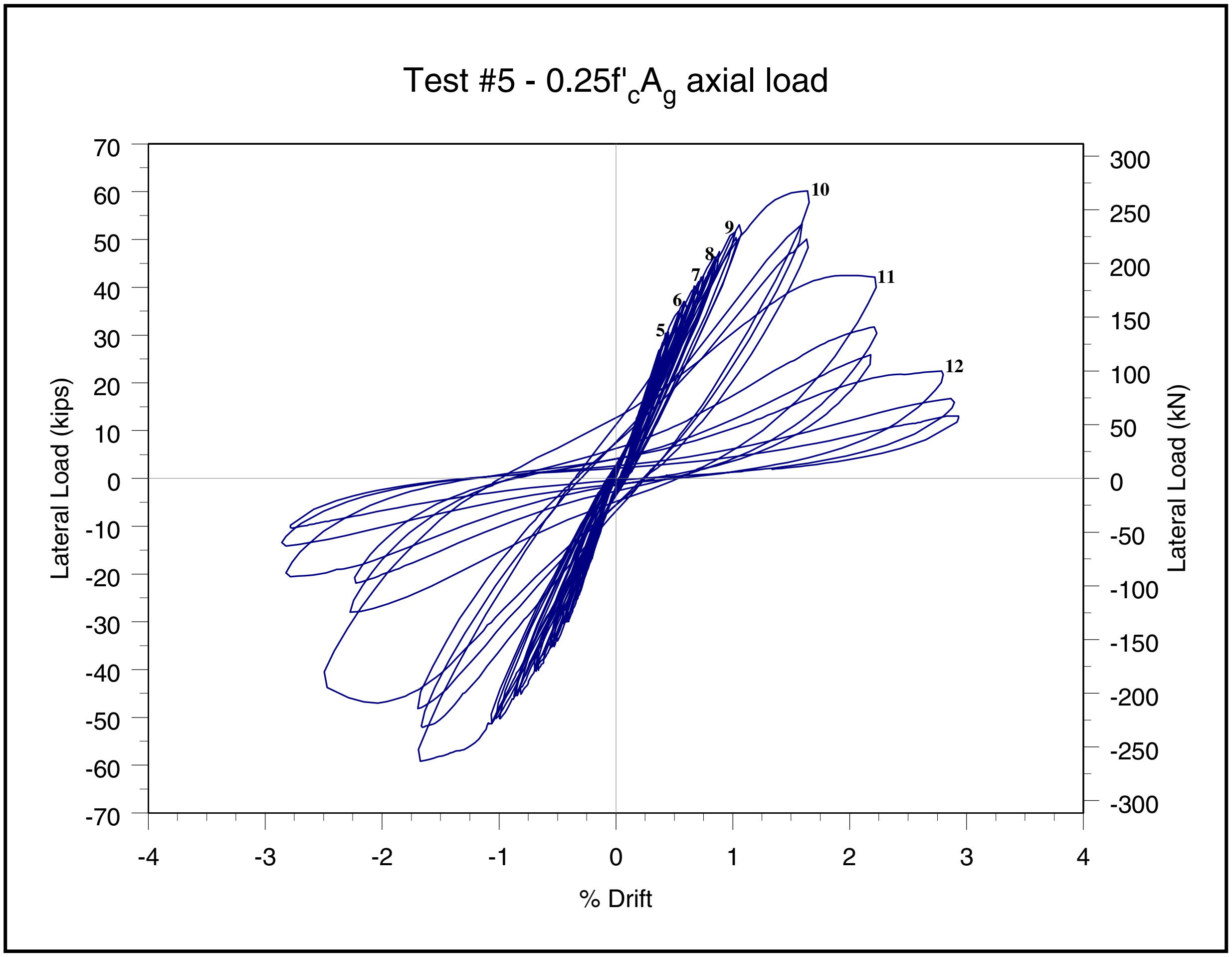

Note: **10** = first cycle of load step number 10

Fig. 4.19 Test #5 load-drift curve

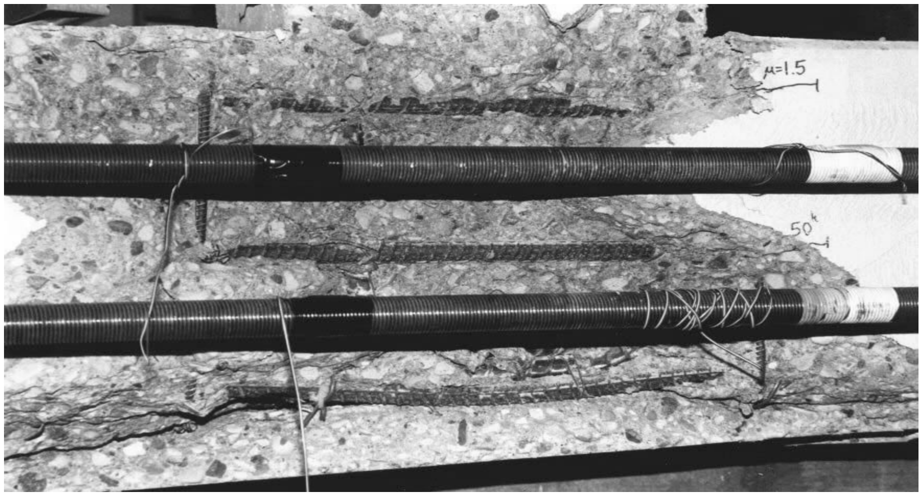

Fig. 4.20 Damage to Test #5 specimen

Ultimate failure of the beam-column specimen is attributed to the development of the limiting joint shear capacity. The joint shear behavior for Test #5 can be seen in Fig. 4.21. The specimen reached a joint shear stress of 985 psi (6.8 MPa), with γ=13.4 (psi) [γ=1.11 (MPa)]. As seen in the diagram, this stress level exceeds that prescribed in both FEMA 273 and ACI 352.

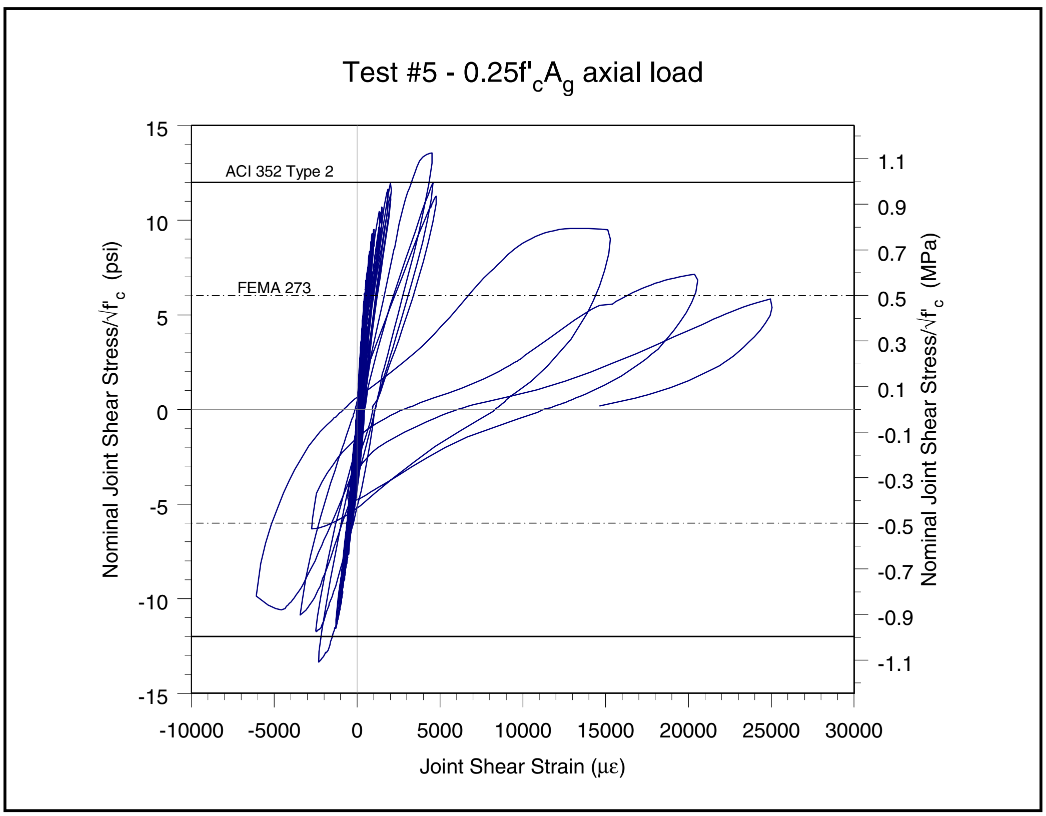

Fig. 4.21 Test #5 joint shear behavior

The maximum nominal joint shear stress occurred at a joint shear strain of 0.003. The response of the column to the cyclic loading is represented by the plots of axial column load shown in Fig. 4.22 and 4.23. The axial compression load in the column was initially set at 305 kips (1357 kN), but due to a shift in the first load step, the axial load was taken to be 319 kips (1419 kN). The column's deteriorating level of axial load is shown in the plots in Fig. 4.22(a) and (b). At the conclusion of the test, the column was holding 257 kips (1143 kN) of compressive load. This is a 19% drop from the original value.

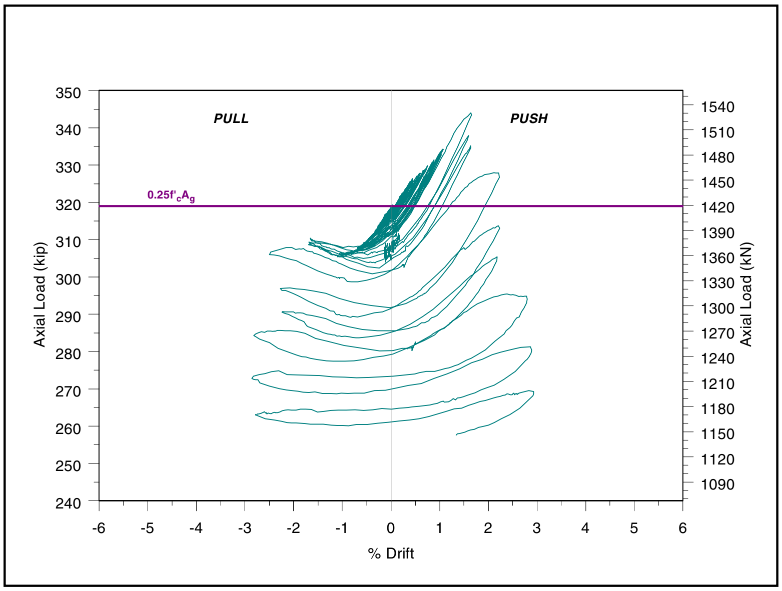

(a)

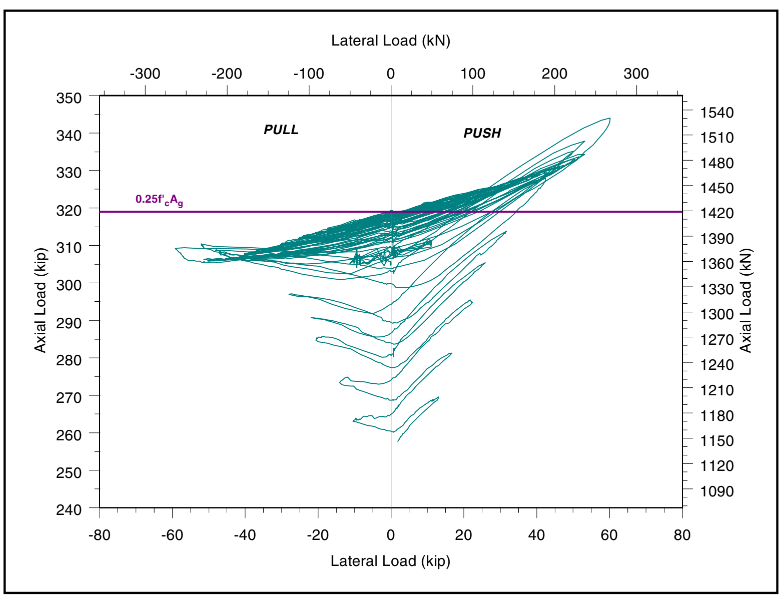

(b)

Fig. 4.22 Test #5 axial load deterioration

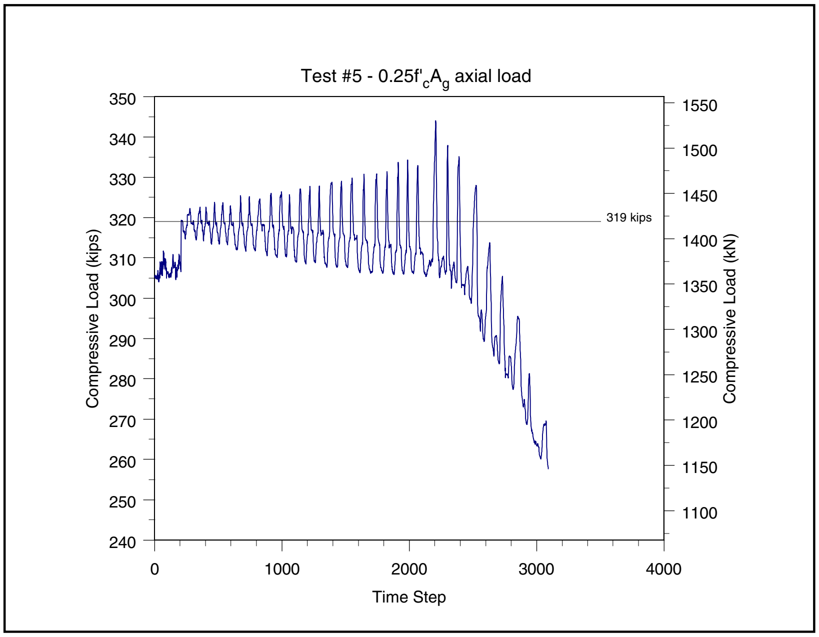

Fig. 4.23 Test #5 column axial load

The amount of energy dissipated in the joint specimen throughout the test is shown in Fig. 4.24. Accelerated energy absorption started at the ninth load step or a drift of 0.9%. The joint dissipated a cumulative 387 k-in. (44 kJ) of energy during the test. The joint had dissipated 19.6% of the total energy at 1% drift and 58.7% of the energy at 2% drift.

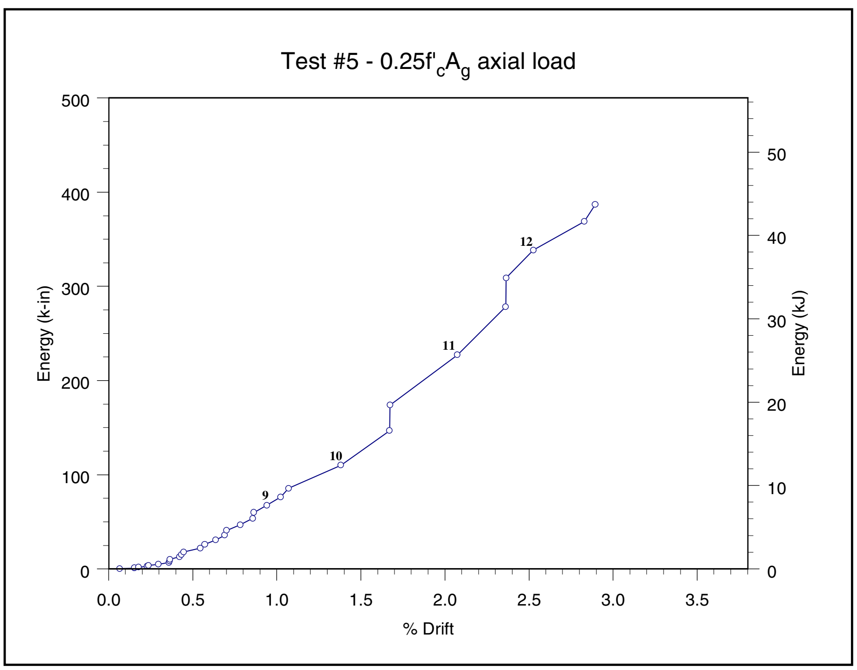

Note: 10 = first cycle of load step number 10

Fig. 4.24 Energy dissipation in Test #5

The beam-column joint specimen in Test #5 was the only specimen that experienced some bar slippage during the test. A column longitudinal bar debonded and slipped at the top of the lap splice region during cyclic loading. This is shown in Fig. 4.25, where the strain versus drift curve remains vertical at drift levels between –2% and 2%. This is where the displacement of the beam is increasing yet the rebar is not receiving any additional strain.

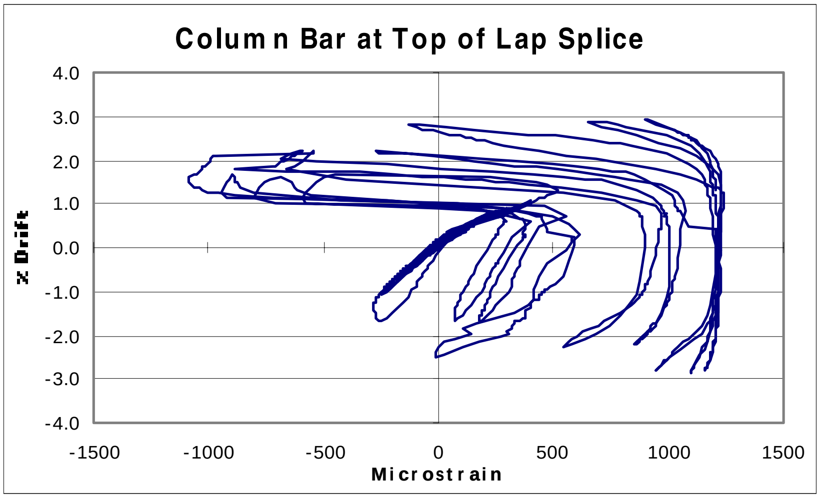

Fig. 4.25 Column bar slippage in Test #5

4.3 COMPARISON OF TESTS WITH 10% AND 25% AXIAL LOAD

All four of the beam-column specimens failed by development of the limiting joint shear capacity. Only a very slight variation in the peak lateral load sustained by each specimen was observed. The level of column axial load compression did not appreciably affect the strength in regard to cyclic load capacity. There is a distinct difference in ductility, however, between the specimens with 10% axial load and those with 25% axial load. Table 4.1 shows that the specimens with the lower axial load were over one and a half times as ductile as the beam-column joints with higher column compression. The lower drift percentage for the specimens with 25% axial load confirms their more relatively brittle character as compared to the 10% axial load specimens.

Table 4.1 Strength and Ductility Comparison

	Axial Load Level		RATIO
	$0.1f'_cA_g$	$0.25f'_cA_g$	$0.1f'_cA_g/0.25f'_cA_g$
Peak Lateral Load	59.5 kips (265 kN)	61 kips (271 kN)	0.98
Absolute Maximum Drift	3.26%	2.55%	1.28
Displacement Ductility	2.7	1.6	1.69

The specimens at the two different axial load levels also showed different joint shear stress behavior. When the joint strength coefficient, γ, is compared for each test, it is obvious that the higher axial column load improved the shear stress capacity of the joint. The average coefficient γ for Test #2 and Test #6, with an axial load of $0.1f'_cA_g$, is 12.4 (psi) [1.03 (MPa)]. For Test #4 and Test#5 with an axial load of $0.25f'_cA_g$, the average maximum γ is 13.4 (psi) [1.11 (MPa)]. The increase is 8% in shear capacity and is a result of increased confinement due to the axial compressive load.

Comparison of the columns' axial load reduction during the tests is inconclusive. The range of capacity loss is too wide a spread between the four specimens to make an accurate statement. For all four columns, the axial load was reduced due to stiffness degradation and concrete cracking in the joint and column; the reduction ranged between 10% and 24%.

The comparison of energy dissipation between the specimens at the two axial load level is represented in Fig. 4.26. The beam-column specimens at the lower axial load level were able to absorb more energy than the specimens with the higher column load. The joints with 10% axial load dissipated on average 474 k-in. (53.6 kJ) of energy, while the joints with 25% axial load only absorbed 378 k-in. (42.7 kJ) of energy. Thus, the specimens with the higher axial load dissipated 20% less energy than the specimens with the smaller level of axial load.

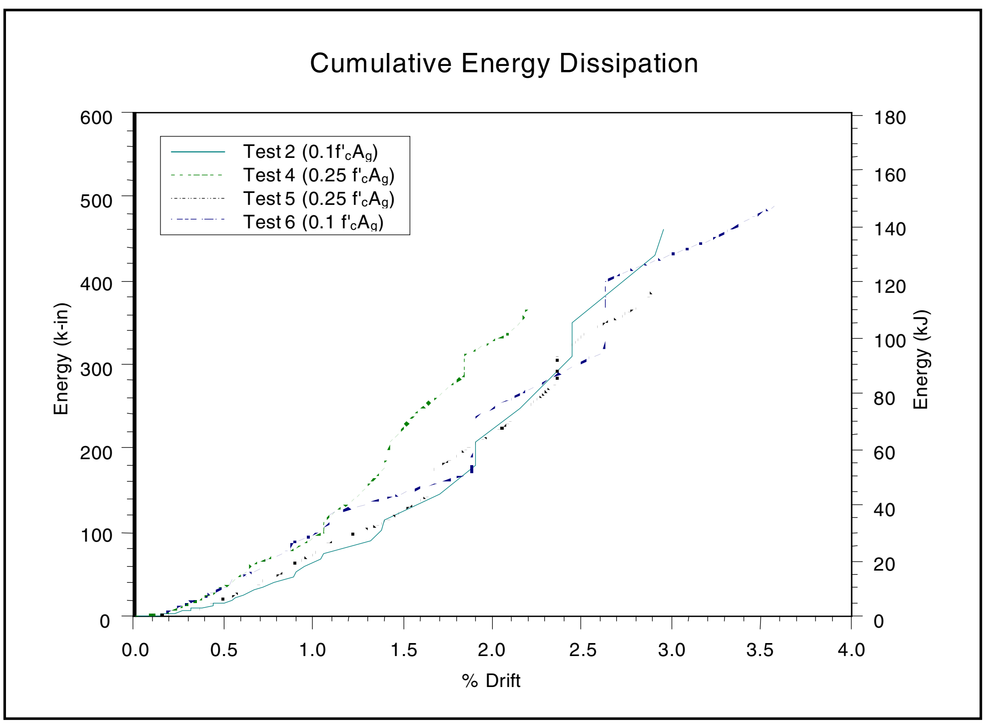

Fig. 4.26 Comparison of energy dissipation

Yielding of the reinforcement always initiated at the beam longitudinal bars. This yielding started earlier in the specimens with the $0.1f'_cA_g$ axial column load, at a drift of 0.5% to 0.6%, whereas for the specimens with the $0.25f'_cA_g$ axial load yielding did not begin until a drift of 0.7% to 1%. Substantial energy dissipation initiated at a drift of 1.1% to 1.3% for the specimens with $0.1f'_cA_g$ column axial load, and a drift of 0.9% for the specimens with $0.25f'_cA_g$ axial load.

The maximum nominal joint shear stress occurred at a joint shear strain between 0.0035 and 0.0045 for the specimens with $0.1f'_cA_g$ column axial load, and in the range of 0.0030 and 0.0035 for the specimens with of $0.25f'_cA_g$ axial load.

5 Performance-Based Evaluation

5.1 DESCRIPTION OF PARAMETERS

Existing performance categories include the FEMA 273 (BSSC 1997) descriptions for buildings and the performance categories developed as part of PEER. The PEER Bridge Performance Database was used as a template in evaluating the performance of the four exterior building joint specimens (Hose, Eberhard, and Seible 2000). A five-level performance evaluation was used based on the analysis of a variety of parameters. These performance categories are well suited for experimental evaluations such as the present study. In addition, for specific subassemblies the parameters included in the performance categories can be expanded with relevant quantities. The parameters in the PEER database include drift, concrete and steel strains, principal stress states, displacement ductility, plastic rotation, curvature ductility, residual deformation index, equivalent viscous damping ratio, and effective stiffness ratio. Explicit procedures on how to calculate these parameters are given in Hose, Eberhard, and Seible (2000). Several other parameters were evaluated, for the four building joint specimens, subsequent to those used for bridges. They included joint shear strain, cumulative dissipated energy, and joint strength coefficient γ. The strength coefficient was calculated as follows:

$$\gamma = \frac{V_n}{\sqrt{f_c^{'}}A_j} \tag{5.1}$$

where V_n = nominal joint shear stress, and A_j = effective horizontal area of the joint. The energy was determined as the area under the force-displacement curves. The joint shear strain was calculated from experimental LVDT strain data using plane strain transformation.

A value for each parameter was calculated at the end of each load step. The results for each of the four specimens are contained in Tables 5.1 through 5.4. These values were used to delineate the five performance levels.

Table 5.1 Test #2 Performance Parameters ($0.1f'_cA_g$)

Load Step	BEAM Steel Strain	COLN Steel Strain	BEAM Concrete Strain *	COLN Concrete Strain *	Curv. Ductility Factor	Plastic Rotation	Principal Comp. Stress	Principal Tension Stress	Drift Ratio	Displ. Ductility Factor	Residual Deform. Index	Equiv. Viscous Damping Ratio	Eff. Stiffness Ratio	Joint Strength Coeff.	Joint Shear Strain	Cum. Energy
	ε_s	ε_s	ε_c	ε_c	μ_ϕ	θ_p	p_c (ksi)	p_t (ksi)	Δ (%)	μ_Δ	RDI	ξ_{eq}	n_k	γ		(k-in.)
1	9.95E-04	9.62E-05	4.94E-04	9.51E-05	0.185	--	-0.049	0.776	0.15	0.141	--	0.107	--	2.3	3.15E-05	1.5
2	1.57E-03	1.92E-04	7.87E-04	1.67E-04	0.300	--	-0.105	0.828	0.24	0.225	--	0.070	--	3.5	1.09E-04	4.1
3	2.05E-03	3.13E-04	9.89E-04	2.56E-04	0.386	--	-0.148	0.891	0.33	0.307	--	0.058	--	4.3	2.51E-04	8.3
4	2.54E-03	5.58E-04	1.27E-03	3.87E-04	0.483	--	-0.215	0.966	0.46	0.426	--	0.046	--	5.4	5.01E-04	14.0
5	2.86E-03	7.52E-04	1.43E-03	4.71E-04	0.544	--	-0.274	1.024	0.57	0.530	--	0.045	--	6.3	7.06E-04	22.4
6	3.41E-03	1.14E-03	1.67E-03	1.44E-03	0.645	--	-0.339	1.110	0.72	0.672	0.07	0.042	--	7.3	1.08E-03	34.6
7	4.05E-03	1.67E-03	2.00E-03	2.52E-03	0.768	--	-0.431	1.193	0.91	0.854	0.09	0.045	--	8.5	1.47E-03	53.0
8	4.76E-03	2.14E-03	2.35E-03	2.16E-03	0.902	--	-0.491	1.302	1.06	0.987	0.10	0.042	1.09	9.5	1.83E-03	74.9
9	5.72E-03	2.42E-03	2.93E-03	1.92E-03	0.995	0.0043	-0.722	1.421	1.44	1.350	0.15	0.052	1.04	11.4	3.09E-03	115.3
10	--	--	--	--	2.166	0.0097	-0.774	1.499	1.91	1.786	0.29	0.079	0.82	12.1	7.18E-03	206.3
11	--	--	--	--	1.620	0.0163	-0.631	1.372	2.47	2.312	0.67	0.128	0.70	10.4	1.34E-02	348.3
12	--	--	--	--	0.803	0.0218	-0.335	1.056	2.95	2.762	0.78	0.118	0.84	6.4	2.87E-02	460.6

*analytically calculated values

Table 5.2 Test #6 Performance Parameters ($0.1f'_cA_g$)

Load Step	BEAM Steel Strain	COLN Steel Strain	BEAM Concrete Strain *	COLN Concrete Strain *	Curv. Ductility Factor	Plastic Rotation	Principal Comp. Stress	Principal Tension Stress	Drift Ratio	Displ. Ductility Factor	Residual Deform. Index	Equiv. Viscous Damping Ratio	Eff. Stiffness Ratio	Joint Strength Coeff.	Joint Shear Strain	Cum. Energy
	ε_s	ε_s	ε_c	ε_c	μ_ϕ	θ_p	p_c (ksi)	p_t (ksi)	Δ (%)	μ_Δ	RDI	ξ_{eq}	n_k	γ		(k-in.)
1	4.87E-04	1.25E-04	4.35E-04	1.34E-04	0.219	--	-0.049	0.668	0.11	0.151	--	0.298	--	2.3	9.50E-05	1.3
2	5.97E-04	1.47E-04	6.70E-04	2.53E-04	0.302	--	-0.147	0.732	0.24	0.350	--	0.245	--	4.0	2.56E-04	6.0
3	1.00E-03	2.06E-04	8.95E-04	3.71E-04	0.452	--	-0.173	0.802	0.32	0.464	--	0.115	--	4.7	4.81E-04	12.8
4	2.01E-03	4.05E-04	1.16E-03	5.37E-04	0.755	--	-0.243	0.852	0.44	0.632	0.11	0.098	--	5.7	6.53E-04	23.4
5	2.60E-03	6.20E-04	1.34E-03	6.35E-04	0.937	--	-0.304	0.901	0.56	0.809	0.11	0.012	--	6.7	9.29E-04	37.2
6	3.36E-03	1.04E-03	1.61E-03	7.89E-04	1.184	0.0002	-0.375	0.987	0.72	1.026	0.14	0.072	1.09	7.8	1.35E-03	55.8
7	3.40E-03	1.74E-03	1.73E-03	9.70E-04	1.221	0.0022	-0.450	1.068	0.88	1.269	0.15	0.060	1.08	8.8	1.78E-03	79.0
8	2.70E-03	2.47E-03	1.71E-03	1.07E-03	1.046	0.0045	-0.537	1.162	1.09	1.560	0.19	0.055	1.06	10.0	2.38E-03	109.7
9	3.29E-03	1.39E-02	--	2.72E-03	1.501	0.0139	-0.790	1.356	1.90	2.722	0.55	0.109	0.72	12.7	4.81E-03	205.4
10	1.38E-03	--	--	--	0.948	0.0225	-0.616	1.187	2.64	3.780	1.24	0.152	0.59	10.5	6.15E-03	366.0
11	1.25E-03	--	--	--	0.552	0.0333	-0.291	0.847	3.57	5.119	1.43	0.129	0.69	6.3	--	488.2

*analytically calculated values

Table 5.3 Test #4 Performance Parameters ($0.25f'_cA_g$)

Load Step	BEAM Steel Strain	COLN Steel Strain	BEAM Concrete Strain *	COLN Concrete Strain *	Curv. Ductility Factor	Plastic Rotation	Principal Comp. Stress	Principal Tension Stress	Drift Ratio	Displ. Ductility Factor	Residual Deform. Index	Equiv. Viscous Damping Ratio	Eff. Stiffness Ratio	Joint Strength Coeff.	Joint Shear Strain	Cum. Energy
	ε_s	ε_s	ε_c	ε_c	μ_ϕ	θ_p	p_c (ksi)	p_t (ksi)	Δ (%)	μ_Δ	RDI	ξ_{eq}	n_k	γ		(k-in.)
1	4.84E-04	8.40E-05	4.32E-04	1.03E-04	0.253	--	-0.027	1.464	0.09	0.116	--	0.083	--	2.4	1.65E-04	1.3
2	6.96E-04	1.18E-04	6.79E-04	1.42E-04	0.380	--	-0.052	1.499	0.13	0.175	--	0.067	--	3.5	2.33E-04	3.5
3	9.73E-04	1.44E-04	8.80E-04	2.03E-04	0.512	--	-0.087	1.531	0.19	0.260	--	0.064	--	4.7	3.93E-04	5.8
4	1.16E-03	1.65E-04	9.86E-04	2.50E-04	0.558	--	-0.124	1.553	0.25	0.330	0.03	0.054	--	5.6	4.98E-04	8.9
5	1.36E-03	2.50E-04	1.03E-03	3.08E-04	0.615	--	-0.166	1.601	0.30	0.405	0.03	0.050	--	6.6	6.37E-04	14.1
6	1.59E-03	4.09E-04	1.40E-03	3.80E-04	1.032	--	-0.223	1.655	0.39	0.522	0.04	0.053	--	7.8	8.47E-04	22.1
7	1.75E-03	5.87E-04	1.33E-03	5.13E-04	0.691	--	-0.292	1.729	0.48	0.647	0.05	0.047	--	9.0	1.11E-03	31.8
8	1.92E-03	9.36E-04	1.54E-03	6.09E-04	0.781	--	-0.344	1.784	0.57	0.774	0.06	0.042	--	10.0	1.46E-03	44.3
9	1.35E-02	1.24E-03	--	6.39E-04	4.818	--	-0.393	1.864	0.66	0.888	0.07	0.043	--	10.9	1.79E-03	60.7
10	1.61E-02	1.60E-02	--	--	5.427	0.0036	-0.593	1.979	1.06	1.424	0.26	0.090	0.81	13.4	3.44E-03	114.4
11	1.52E-02	1.53E-02	--	--	1.452	0.0080	-0.580	1.972	1.43	1.931	0.44	0.109	0.74	13.2	8.45E-03	207.6
12	--	--	--	--	2.091	0.0128	-0.350	1.747	1.84	2.485	0.89	0.156	0.66	9.4	2.64E-02	310.4
13	--	--	--	--	1.267	0.0169	-0.135	1.372	2.20	2.964	0.88	0.127	0.99	5.0	5.69E-04	369.6

*analytically calculated values

Table 5.4 Test #5 Performance Parameters ($0.25f'_cA_g$)

Load Step	BEAM Steel Strain	COLN Steel Strain	BEAM Concrete Strain *	COLN Concrete Strain *	Curv. Ductility Factor	Plastic Rotation	Principal Comp. Stress	Principal Tension Stress	Drift Ratio	Displ. Ductility Factor	Residual Deform. Index	Equiv. Viscous Damping Ratio	Eff. Stiffness Ratio	Joint Strength Coeff.	Joint Shear Strain	Cum. Energy
	ε_s	ε_s	ε_c	ε_c	μ_ϕ	θ_p	p_c (ksi)	p_t (ksi)	Δ (%)	μ_Δ	RDI	ξ_{eq}	n_k	γ		(k-in.)
1	5.03E-04	1.35E-04	4.76E-04	9.63E-05	0.197	--	-0.024	1.478	0.15	0.089	--	0.072	--	2.5	2.11E-04	1.2
2	7.38E-04	2.22E-04	7.87E-04	1.67E-04	0.289	--	-0.055	1.545	0.24	0.139	--	0.057	--	3.9	3.15E-04	3.7
3	9.29E-04	3.10E-04	9.86E-04	2.41E-04	0.352	--	-0.082	1.581	0.30	0.173	--	0.043	--	4.8	3.85E-04	6.6
4	1.14E-03	4.20E-04	9.16E-04	3.33E-04	0.442	--	-0.125	1.631	0.36	0.213	0.016874	0.044	--	5.9	4.94E-04	10.0
5	1.29E-03	5.05E-04	1.43E-03	4.71E-04	0.530	--	-0.158	1.665	0.45	0.261	0.021314	0.050	--	6.9	6.01E-04	15.3
6	1.57E-03	7.04E-04	1.60E-03	5.62E-04	0.676	--	-0.216	1.733	0.58	0.342	0.03	0.053	--	8.2	7.97E-04	26.0
7	1.82E-03	9.68E-04	2.00E-03	2.52E-03	0.868	--	-0.270	1.798	0.72	0.422	0.03	0.046	--	9.3	1.03E-03	40.9
8	2.04E-03	1.31E-03	2.35E-03	2.16E-03	1.044	--	-0.329	1.864	0.88	0.513	0.04	0.041	--	10.5	1.51E-03	59.8
9	2.28E-03	1.66E-03	2.71E-03	2.93E-03	1.221	--	-0.396	1.943	1.07	0.625	0.05	0.039	--	11.8	2.10E-03	85.5
10	6.36E-03	7.90E-03	--	--	2.067	--	-0.496	2.069	1.67	0.977	0.18	0.095	0.97	13.4	4.84E-03	174.0
11	--	--	--	--	1.943	0.0075	-0.341	1.791	2.36	1.380	0.36	0.128	0.80	10.1	5.85E-02	308.9
12	--	--	--	--	1.243	0.0137	-0.094	1.459	2.90	1.691	0.54	0.142	0.64	4.8	5.85E-02	386.8

*analytically calculated values

5.2 PERFORMANCE LEVELS

Five levels of performance were used to characterize the joints. These levels were determined based on the evaluation and comparison of the previously tabulated parameters. After analysis of the four joint specimens, the governing parameters for delineating between performance levels were found to be drift, joint crack width, and the joint strength coefficient γ. The type of damage associated with each step was also used as a parameter for determining the performance levels. The performance level boundaries are slightly different for the two levels of axial column load. Table 5.5 summarizes the characteristics of each performance level.

Table 5.5 Performance Levels in Terms of Critical Parameters

(a) $0.1f'_cA_g$

Performance Level	Drift %	Crack Width in. (mm)	γ psi (MPa)
I	0.24	--	3.7 (0.31)
II	0.56	hairline	6.5 (0.54)
III	0.9	0.004 (0.1)	8.6 (0.71)
IV	1.9	0.05 (1.2)	12.4 (1.03)
V	2.5	≥0.18 (4.5)	10.5 (0.87)

(b) $0.25f'_cA_g$

Performance Level	Drift %	Crack Width in. (mm)	γ psi (MPa)
I	0.25	--	4.7 (0.39)
II	0.46	hairline	7.9 (0.66)
III	0.7	0.004 (0.1)	10.7 (0.89)
IV	1.5	0.10 (2.5)	13.3 (1.10)
V	2.0	≥0.33 (8.5)	9.7 (0.81)

Level I showed no damage to the joint specimen and occurred at very low levels of drift. Level II was characterized by barely visible, initial cracking in the joint. The first yielding of longitudinal reinforcement occurred in this performance level. Level III showed growing diagonal cracks in the joint and the appearance of more cracks in the beam and joint. This level represents the initial stages of the failure mechanism. Level IV occurred at the peak lateral load. Extensive cracking in the joint and the extension of diagonal joint cracks into the column was seen in this performance level. This stage represents full development of the failure mechanism. Level V was characterized by lateral load strength degradation and spalling concrete on the back of the column at the joint.

The performance levels with detailed descriptions are shown for each beam-column joint specimen in Tables 5.6 to 5.9. The performance levels are also marked on each joint respective hysteretic-envelope curve in Figures 5.1, 5.3, 5.5, and 5.7. Photographic documentation was done on each test for all five performance levels and is presented in Figures 5.2, 5.4, 5.6, and 5.8.

Table 5.6 Test #2 Performance Levels ($0.1f'_cA_g$)

Level	Qualitative Performance Description	Quantitative Performance Description	Load Step	Lateral Load kip (kN)	Crack Width in (mm)	Drift %	γ psi (MPa)
I	no damage	--	2	17 (76)	--	0.24	3.5 (0.29)
II	first yield in longitudinal reinforcement	--	5	31 (138)	hairline	0.57	6.3 (0.52)
III	initiation of mechanism	initial cracking in the joint and beam	7	42 (187)	0.004 (0.1)	0.91	8.5 (0.71)
IV	formation of local mechanism	extensive shear cracking in joint, joint shear cracks extending into column, continued cracking in the beam	10	60 (267)	0.04 (1.12)	1.91	12.1 (1.00)
V	strength degradation	spalling concrete in the joint and back of the column	11	52 (231)	0.18 (4.5)	2.47	10.4 (0.86)

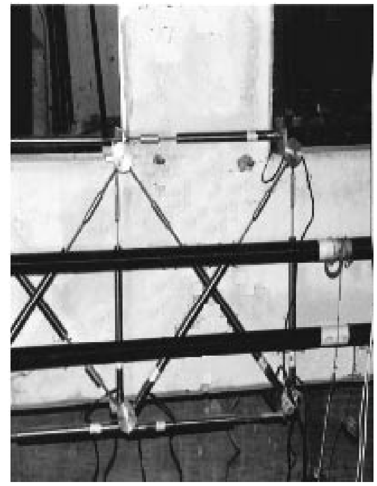

Level I

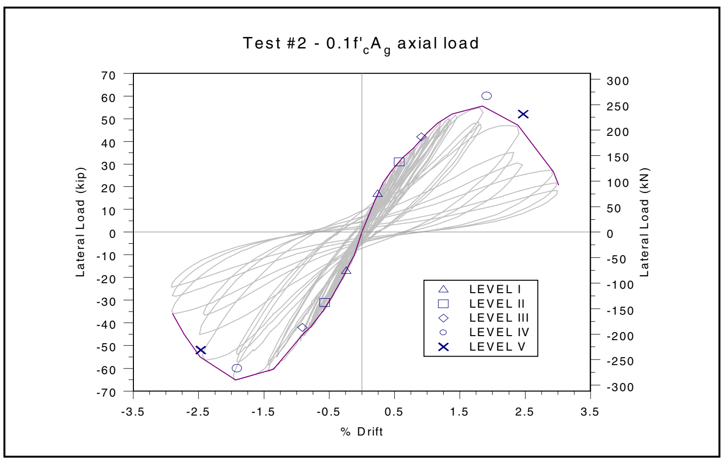

Fig. 5.1 Test #2 performance level identification curve

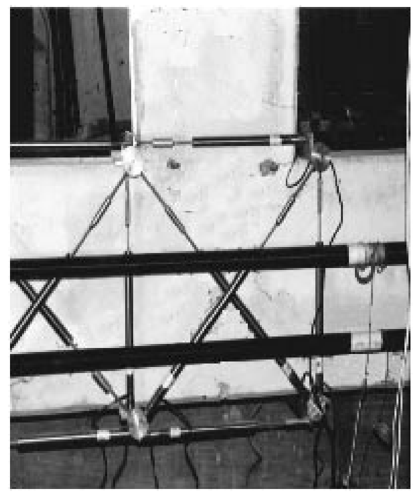

Level II

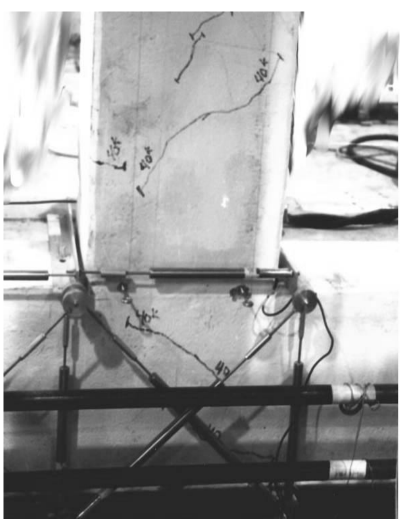

Level III

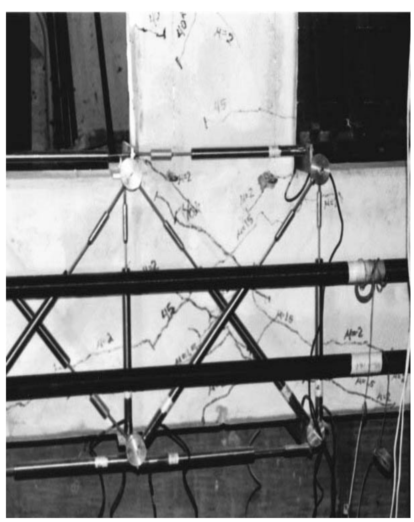

Level IV

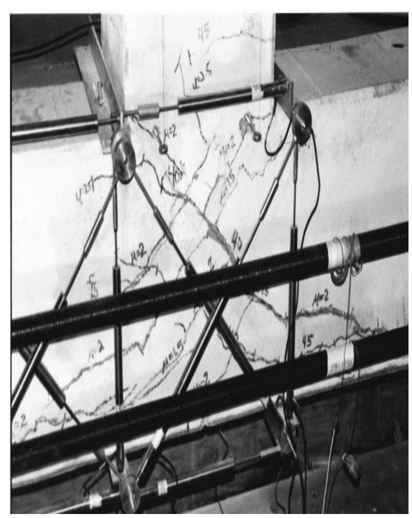

Level V

Fig. 5.2 Test #2 photo documentation of performance levels

Table 5.7 Test #6 Performance Levels ($0.1f'_cA_g$)

Level	Qualitative Performance Description	Quantitative Performance Description	Load Step	Lateral Load kip (kN)	Crack Width in (mm)	Drift %	γ psi (MPa)
I	no damage	--	2	18 (80)	--	0.24	4.0 (0.33)
II	first yield in longitudinal reinforcement	onset of cracking in the joint and beam	5	31 (138)	hairline	0.56	6.7 (0.56)
III	initiation of mechanism	continued cracking in the beam and beam/column interface	7	41 (182)	0.004 (0.1)	0.88	8.8 (0.73)
IV	formation of local mechanism	extensive shear cracking in the joint, diagonal joint cracks extend into the column	9	59 (262)	0.06 (1.4)	1.90	12.7 (1.05)
V	strength degradation	spalling concrete in the joint and back of column	10	49 (218)	0.79 (20)	2.64	10.5 (0.87)

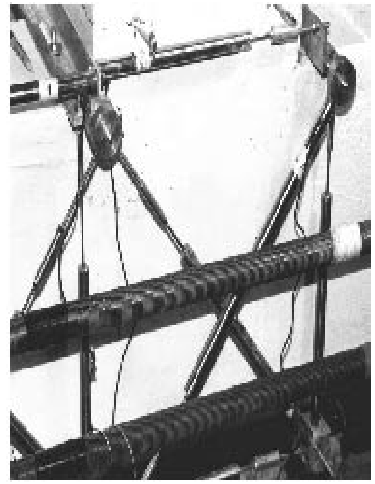

Level I

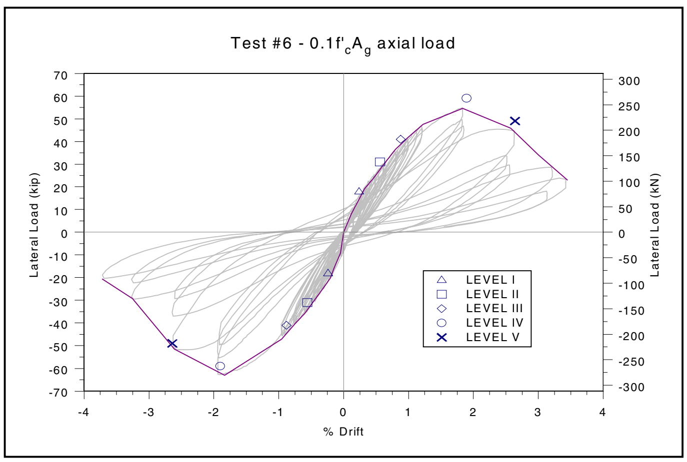

Fig. 5.3 Test #6 performance level identification curve

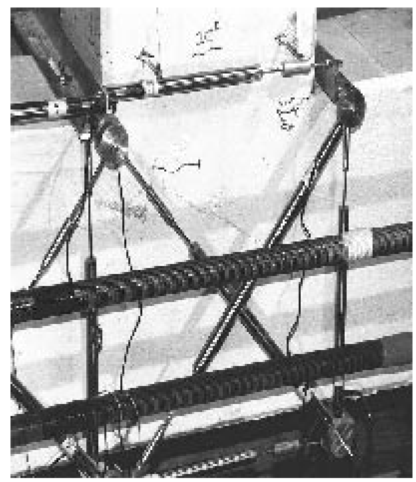

Level II

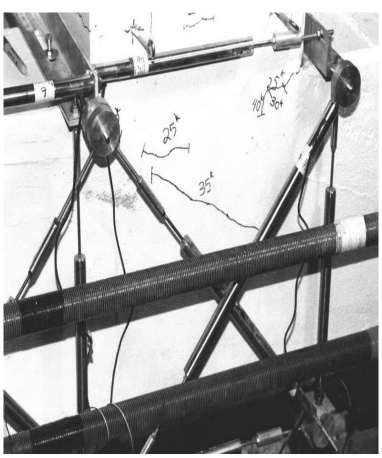

Level III

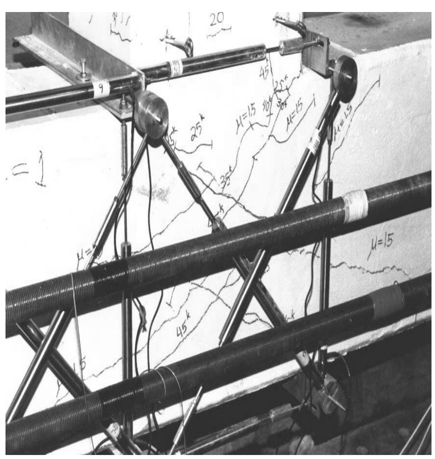

Level IV

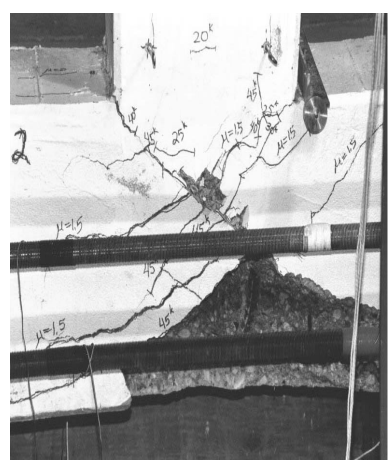

Level V

Fig. 5.4 Test #6 photo documentation of performance levels

Table 5.8 Test #4 Performance Levels ($0.25f'_cA_g$)

Level	Qualitative Performance Description	Quantitative Performance Description	Load Step	Lateral Load kip (kN)	Crack Width in (mm)	Drift %	γ psi (MPa)
I	no damage	barely visible cracking in beam and joint	4	26 (116)	--	0.25	5.6 (0.46)
II	initiation of mechanism	onset of shear cracking in the joint, continued cracking in the beam	7	42 (187)	hairline	0.48	9.0 (0.75)
III	first yield in longitudinal reinforcement	growing diagonal cracks in the joint	9	51 (227)	0.004 (0.1)	0.66	10.9 (0.91)
IV	formation of local mechanism	diagonal joint cracks extending into the column	11	61 (271)	0.14 (3.5)	1.43	13.2 (1.10)
V	strength degradation	spalling concrete in joint and back of column	12	44 (196)	0.35 (9)	1.84	9.4 (0.78)

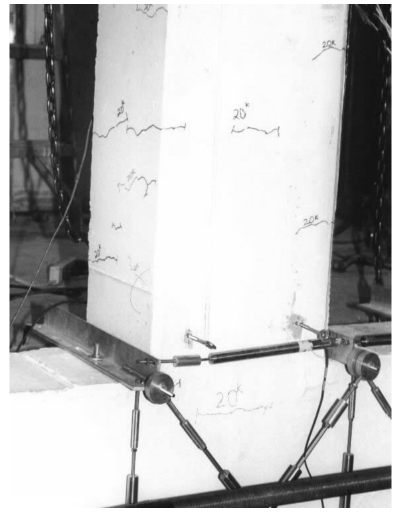

Level I

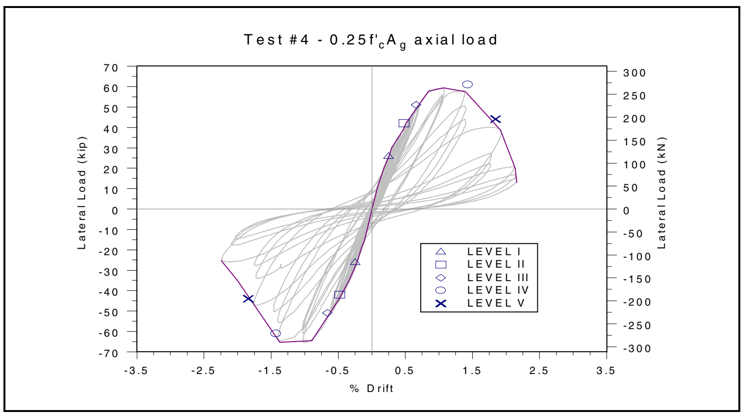

Fig. 5.5 Test #4 performance level identification curve

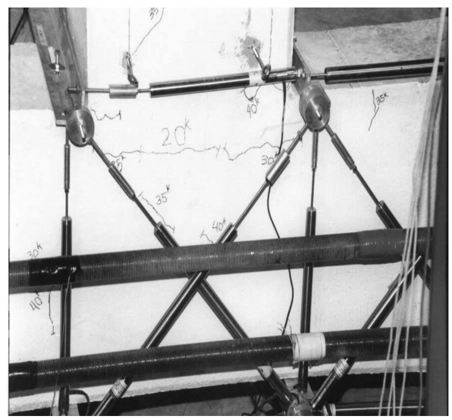

Level II

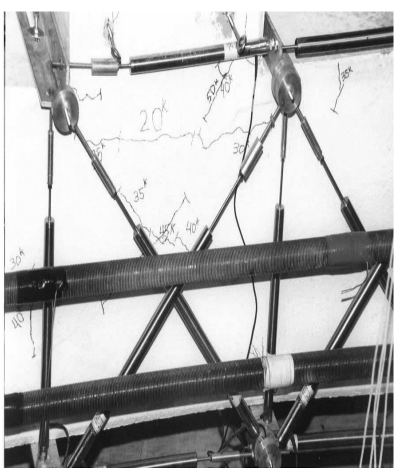

Level III

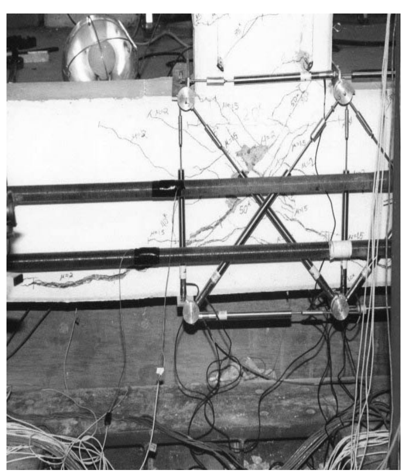

Level IV

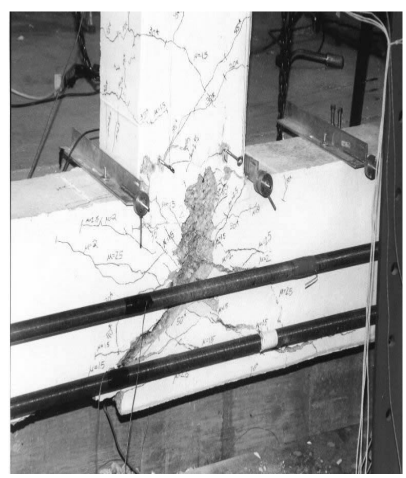

Level V

Fig. 5.6 Test #4 photo documentation of performance levels

Table 5.9 Test #5 Performance Levels ($0.25f'_cA_g$)

Level	Qualitative Performance Description	Quantitative Performance Description	Load Step	Lateral Load kip (kN)	Crack Width in (mm)	Drift %	γ psi (MPa)
I	no damage	--	2	17 (76)	--	0.24	3.9 (0.32)
II	--	cracking in the beam, barely visible cracking in the joint	5	31 (138)	hairline	0.45	6.9 (0.57)
III	--	growing shear cracks in the joint, continued cracking in the beam	8	47 (209)	0.005 (0.12)	0.88	10.5 (0.87)
IV	first yield in longitudinal reinforcement	extensive shear cracking in the joint, diagonal cracks extend into the column	10	60 (267)	0.06 (1.5)	1.67	13.4 (1.11)
V	strength degradation	buckling of longitudinal column bars at back of column, spalling concrete in joint and back of column	11	45 (200)	0.33 (8.5)	2.36	10.1 (0.84)

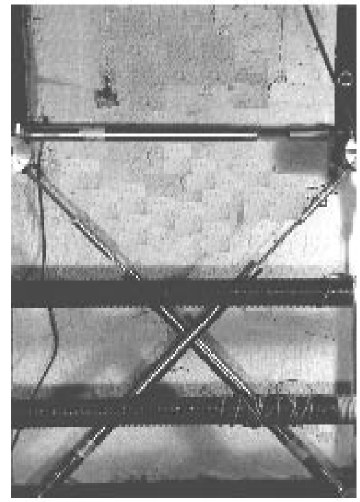

Level I

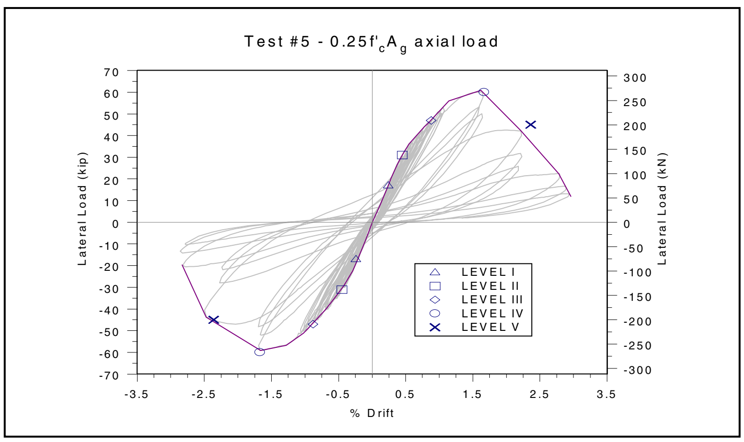

Fig. 5.7 Test #5 performance level identification curve

Level II

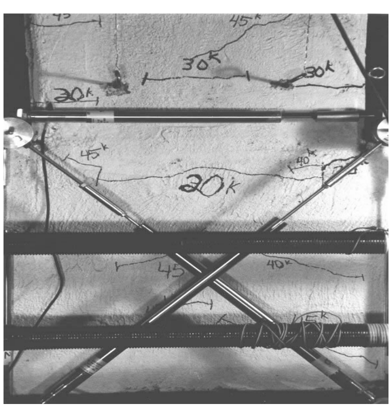

Level III

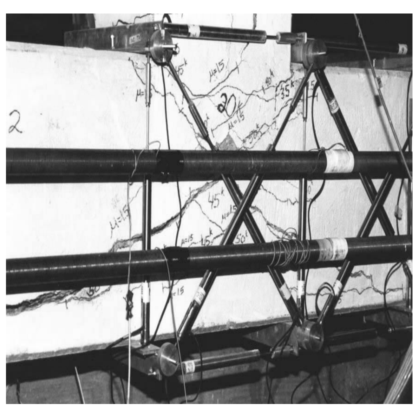

Level IV

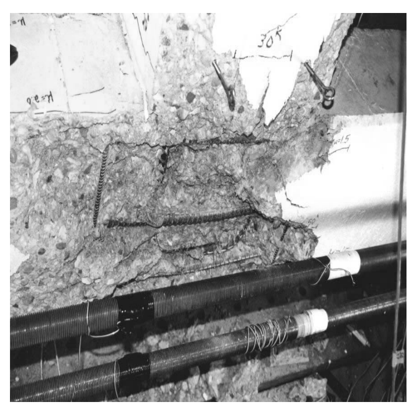

Level V

Fig. 5.8 Test #5 photo documentation of performance levels

It should be noted that these performance levels are based only on four joint tests. The parameters are average values. Subsequent studies are needed to further substantiate the findings in this report and solidify the performance level delineation. Since this is solely an engineering study, socio-economic descriptions were not assigned to the five performance levels. This latter type of classification is expected to be developed in cooperation with the social scientists involved in PEER.

5.3 COMPARISON WITH FEMA 273 AND ACI 352

The joints tested for this research do not qualify as either Type I or Type II joints per ACI 352 (ACI 1991) since the reinforcement is of Type I but the loading is of Type II. However, a comparison was made of the test results with the FEMA 273 (BSSC 1997) modeling parameters for reinforced concrete beam-column joints. Specifically, the shear angle parameters at the end of the peak strength (d) and at the collapse level (e), and the residual strength ratio, as defined in Fig. 5.9, were compared to Table 6-8 of FEMA 273. FEMA 273 parameters do not exist for an axial load ratio of 0.25. However, Table 5.10 shows that for an axial load ratio of $0.1f'_cA_g$ the FEMA Guidelines are conservative.

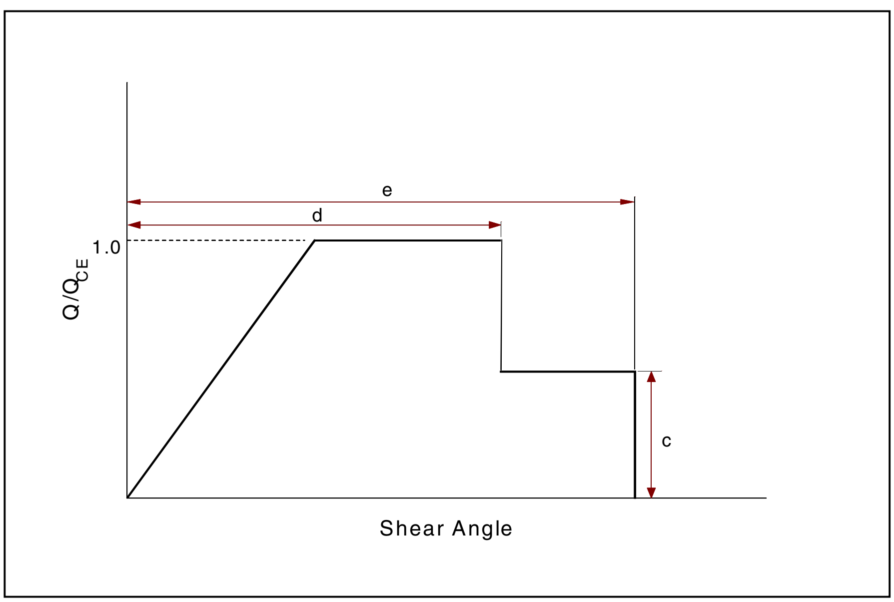

Fig. 5.9 FEMA modeling parameters

Table 5.10 Modeling Parameters for Specimens in Comparison with FEMA 273

Test #	P/f'_cA_g [1]	Transverse Reinforcement	V/V_n [2]	d	e	c
2	0.10	NC [3]	0.57	0.023	0.030	0.449
6	0.10	NC	0.59	0.025	0.034	0.480
4	0.25	NC	0.62	0.014	0.021	0.489
5	0.25	NC	0.63	0.016	0.029	0.598
FEMA 273	≤ 0.1	NC [4]	≤ 1.2	0.005	0.010	0.200

[1] ratio of the axial column load to the cross-sectional area of the joint and concrete compressive strength
[2] ratio of the design shear force to the shear strength for the joint: V_n is calculated using Equation 6-4 in FEMA 273 Section 5.5.2.3
[3] nonconforming details; no hoops within the joint
[4] nonconforming details; see Table 6-8 footnote 1. of FEMA 273

In terms of the shear strength coefficient, γ, the FEMA 273 Guidelines suggest a value of $\gamma = 6$ (psi) or 0.5 (MPa) for exterior joints without transverse beams. This is very conservative for the present joint specimens, since this research has shown that for the case of an axial column load of $0.1f'_cA_g$,the coefficient $\gamma = 12.4$ (psi) or 1.03 (MPa), and that for a column axial load of $0.25f'_cA_g$,the coefficient $\gamma = 13.4$ (psi) or 1.11 (MPa).

Comparing the results for the shear strength coefficient obtained in this research to the coefficient suggested by ACI 352 for new joints, which is $\gamma = 12$ (psi) or 1.0 (MPa), it can be observed that even nonductile joints without hoop steel in the joint can meet this design value. This is true for the joints tested here with the reinforcement details described in Chapter 2 and at both the $0.1f'_cA_g$ axial column load and $0.25f'_cA_g$ axial load levels.

The specimens with $0.1f'_cA_g$ axial load had a maximum equivalent viscous damping ratio in the range of 12.8% to 15.2%, whereas the specimens with $0.25f'_cA_g$ axial load had a maximum equivalent viscous damping ratio in the range of 12.8% to 15.6%.

6 Conclusions

This investigation has shown that several performance levels can be delineated in terms of the reinforced concrete nonductile building joints that were tested. These performance levels have been categorized for two levels of axial column compression load in terms of drift, joint strength coefficient, and crack width. One of the findings of this study is that the joint strength coefficient, γ, changes with the variation of the column compressive axial load. For the joints with $0.1f'_cA_g$ axial load in the column, the value of γ was 12.4 (psi) or 1.03 (MPa). For joints with $0.25f'_cA_g$ axial load in the column, the value of γ was 13.4 (psi) or 1.11 (MPa), which is an increase of 8%. The FEMA 273 (BSSC 1997) joint shear strength coefficient is given as $\gamma = 6$ (psi) or 0.5 (MPa) for existing exterior joints without transverse beams, which is seen to be very conservative when compared with the results of this research. The ACI 352 (1991) joint shear strength coefficient for new Type II exterior joints is given as $\gamma = 12$ (psi) or 1.0 (MPa), which was actually met by the joints tested in this research for both axial column loads of $0.1f'_cA_g$ and $0.25f'_cA_g$.

The maximum nominal joint shear stress occurred at a joint shear strain between 0.0035 and 0.0045 for the specimens with $0.1f'_cA_g$ column axial load, and in the range of 0.0030 and 0.0035 for the specimens with of $0.25f'_cA_g$ axial load. The principal tensile stress in the joint for the specimens with $0.1f'_cA_g$ axial column load was on average $18\sqrt{f'_c}$ (psi) or $1.5\sqrt{f'_c}$ (MPa), whereas for the specimens with an axial load of $0.25f'_cA_g$ column load, the principal tensile stress was $27\sqrt{f'_c}$ (psi) or $2.24\sqrt{f'_c}$ (MPa); this is an increase of 50% in the principal tensile stresses. The results have also indicated that the FEMA 273 (BSSC 1997) modeling parameters for seismic rehabilitation of joints are conservative.

The joints with $0.1f'_cA_g$ axial compressive loading in the columns experienced a drop of 10% to 24% of the axial load, at drifts of 3% to 3.5%. The joints with $0.25f'_cA_g$ axial compression in the column experienced a drop of 17% to 19% of the axial load, at drifts of 2.2%

to 2.9%. Due to the loading setup and test procedure, this drop in the axial column load can not be taken to mean that the axial capacity of the column was reduced; nevertheless, the drop in the axial load represents the loss of stiffness due to progressive cracking in the joint and column at higher drift levels.

In terms of energy dissipation, the specimens with $0.25f'_cA_g$ axial load dissipated an average of 20% less energy than the specimens with $0.1f'_cA_g$ axial load. Substantial energy dissipation initiated at a drift of 1.2% for the specimens with $0.1f'_cA_g$ column axial load, and a drift of 0.9% for the specimens with $0.25f'_cA_g$ axial load.

The displacement ductility of the specimens with the $0.1f'_cA_g$ column load was on average 2.7 as compared to 1.6 for the specimens with $0.25f'_cA_g$ axial column compressive load. Yielding of the reinforcement always initiated at the beam longitudinal bars and started earlier in the specimens with the $0.1f'_cA_g$ axial column load, at a drift of 0.5% to 0.6%, whereas for the specimens with the $0.25f'_cA_g$ axial load, yielding did not begin until a drift of 0.7% to 1%.

REFERENCES

ACI Committee 352. 1991. *Recommendations for design of beam-column joints in monolithic reinforced concrete structures* (ACI 352R-91). Farmington Hills, Mich.: American Concrete Institute.

Beres, A., A. N. White, and P. Gergely. 1992. *Seismic behavior of RC frame structures with nonductile details: Part I-Summary of experimental findings of full scale beam-column joint tests.* Report NCEER-92-0024. Buffalo, N.Y.: NCEER, SUNY.

Building Seismic Safety Council. 1997. FEMA 273: *NEHRP Guidelines for the seismic rehabilitation of buildings*. Washington, D.C.: Federal Emergency Management Agency.

Durrani, A. J., and H. E. Zerbe. 1987. *Seismic resistance of R/C exterior connections with floor slab. J. of Structural Engineering* 113(8): 1850–64.

Ehsani, M. R., and J. K. Wight. 1985. Exterior reinforced concrete beam-to-column connections subjected to earthquake-type loading. *ACI Journal* 492–9.

Hose, Yael D., M. Eberhard, and F. Seible. 1999. *Performance library of concrete bridge components, sub-assemblages and systems under simulated seismic Loads*. SSRP 99/08. La Jolla, Calif.: Structural Systems Research Program, University of California, San Diego.

Kurose, Y. 1987. *Recent studies on reinforced concrete beam column joints in Japan*. PMFSEL Report No. 87–8. Austin, Texas: Department of Civil Engineering , University of Texas at Austin.

Megget, L. M. 1974. Cyclic behaviour of exterior reinforced concrete beam-column joints. *Bull. of the New Zealand National Society for Earthquake Engineering* 7(1).

Pantazapoulou, S. J., and J. F. Bonacci. 1992. Consideration of questions about beam-column joints. *ACI Structural Journal* 89(1), 27–36.

Pantazapoulou, S. J., and J. F. Bonacci. 1994. On earthquake-resistant reinforced concrete frame connections. *Canadian J. of Civil Engineering* 21: 307–28.

Park, R. 1997. *New Zealand Code Developments in the Design and Construction of Reinforced Concrete Moment Resisting Frames for Earthquake Resistance*. UCB/EERC-97/05, 9–16. Berkeley, Calif.: Earthquake Engineering Research Center, University of California.

Paulay, T., and A. Scarpas. 1981. The behaviour of exterior beam-column joints. *Bull. of the New Zealand National Society for Earthquake Engineering* 14(3): 131–44.

Townsend, W. H., and R. D. Hanson. 1977. Reinforced concrete connection hysteresis loops. ACI Publication SP53-13. *Reinforced Concrete Structures in Seismic Zones,* 351–70.

Tsonos, A. G., I. A. Tegos, and G. G. Penelis. 1995. Influence of axial force variations on the seismic behavior of exterior beam-column joints. European Earthquake Engineering 3: 51–63.

Uzumeri, S. M. 1977. Strength and ductility of cast-in-place beam-column joints. ACI Publication SP 53-12. *Reinforced Concrete Structures in Seismic Zones*, 293–350.

PEER REPORTS

PEER reports are available from the National Information Service for Earthquake Engineering (NISEE). To order PEER reports, please contact the Pacific Earthquake Engineering Research Center, 1301 South 46th Street, Richmond, California 94804-4698. Tel.: (510) 231-9468; Fax: (510) 231-9461.

PEER 2000/07 *Cover-Plate and Flange-Plate Reinforced Steel Moment-Resisting Connections.* Taejin Kim, Andrew S. Whittaker, Amir S. Gilani, Vitelmo V. Bertero, and Shakhzod M. Takhirov. September …9.';2000. $33.00

PEER 2000/06 *Seismic Evaluation and Analysis of 230-kV Disconnect Switches.* Amir S. J. Gilani, Andrew S. Whittaker, Gregory L. Fenves, Chun-Hao Chen, Henry Ho, and Eric Fujisaki. July 2000. $26.00

PEER 2000/04 *An Evaluation of Seismic Energy Demand: An Attenuation Approach.* Chung-Che Chou and Chia-Ming Uang. July 1999. $20.00

PEER 2000/03 *Framing Earthquake Retrofitting Decisions: The Case of Hillside Homes in Los Angeles.* Detlof von Winterfeldt, Nels Roselund, and Alicia Kitsuse. March 2000. $13.00

PEER 2000/01 *Further Studies on Seismic Interaction in Interconnected Electrical Substation Equipment.* Armen Der Kiureghian, Kee-Jeung Hong, and Jerome L. Sackman. November 1999. $20.00

PEER 1999/14 *Seismic Evaluation and Retrofit of 230-kV Porcelain Transformer Bushings*. Amir S. Gilani, Andrew S. Whittaker, Gregory L. Fenves, and Eric Fujisaki. December 1999. $26.00

PEER 1999/12 *Rehabilitation of Nonductile RC Frame Building Using Encasement Plates and Energy-Dissipating Devices.* Mehrdad Sasani, Vitelmo V. Bertero, James C. Anderson. December 1999. $26.00

PEER 1999/11 *Performance Evaluation Database for Concrete Bridge Components and Systems under Simulated Seismic Loads.* Yael D. Hose and Frieder Seible. November 1999. $20.00

PEER 1999/10 *U.S.-Japan Workshop on Performance-Based Earthquake Engineering Methodology for Reinforced Concrete Building Structures.* December 1999. $33.00

PEER 1999/09 *Performance Improvement of Long Period Building Structures Subjected to Severe Pulse-Type Ground Motions*. James C. Anderson, Vitelmo V. Bertero, and Raul Bertero. October 1999. $26.00

PEER 1999/08 *Envelopes for Seismic Response Vectors.* Charles Menun and Armen Der Kiureghian. July 1999. $26.00

PEER 1999/07 *Documentation of Strengths and Weaknesses of Current Computer Analysis Methods for Seismic Performance of Reinforced Concrete Members.* William F. Cofer. November 1999. $15.00

PEER 1999/06 *Rocking Response and Overturning of Anchored Equipment under Seismic Excitations.* Nicos Makris and Jian Zhang. November 1999. $15.00

PEER 1999/05 *Seismic Evaluation of 550 kV Porcelain Transformer Bushings.* Amir S. Gilani, Andrew S. Whittaker, Gregory L. Fenves, and Eric Fujisaki. October 1999. $15.00

PEER 1999/04 *Adoption and Enforcement of Earthquake Risk-Reduction Measures.* Peter J. May, Raymond J. Burby, T. Jens Feeley, and Robert Wood. $15.00

PEER 1999/03 *Task 3 Characterization of Site Response General Site Categories*. Adrian Rodriguez-Marek, Jonathan D. Bray, and Norman Abrahamson. February 1999. $20.00

PEER 1999/02 *Capacity-Demand-Diagram Methods for Estimating Seismic Deformation of Inelastic Structures: SDF Systems*. Anil K. Chopra and Rakesh Goel. April 1999. $15.00

PEER 1999/01 *Interaction in Interconnected Electrical Substation Equipment Subjected to Earthquake Ground Motions.* Armen Der Kiureghian, Jerome L. Sackman, and Kee-Jeung Hong. February 1999. $20.00

PEER 1998/08 *Behavior and Failure Analysis of a Multiple-Frame Highway Bridge in the 1994 Northridge Earthquake.* Gregory L. Fenves and Michael Ellery. December 1998. $20.00

PEER 1998/07 *Empirical Evaluation of Inertial Soil-Structure Interaction Effects.* Jonathan P. Stewart, Raymond B. Seed, and Gregory L. Fenves. November 1998. $26.00

PEER 1998/06 *Effect of Damping Mechanisms on the Response of Seismic Isolated Structures.* Nicos Makris and Shih-Po Chang. November 1998. $15.00

PEER 1998/05 *Rocking Response and Overturning of Equipment under Horizontal Pulse-Type Motions.* Nicos Makris and Yiannis Roussos. October 1998. $15.00

PEER 1998/04 *Pacific Earthquake Engineering Research Invitational Workshop Proceedings, May 14–15, 1998: Defining the Links between Planning, Policy Analysis, Economics and Earthquake Engineering.* Mary Comerio and Peter Gordon. September 1998. $15.00

PEER 1998/03 *Repair/Upgrade Procedures for Welded Beam to Column Connections.* James C. Anderson and Xiaojing Duan. May 1998. $33.00

PEER 1998/02 *Seismic Evaluation of 196 kV Porcelain Transformer Bushings.* Amir S. Gilani, Juan W. Chavez, Gregory L. Fenves, and Andrew S. Whittaker. May 1998. $20.00

PEER 1998/01 Unassigned.